Spring 2023

Area Average Surface Transfer Coefficient in Unit Cell Geometries

Benjamin Gabriel Mackey
Missouri University of Science and Technology

Department:

AREA AVERAGE SURFACE TRANSFER COEFFICIENTS IN UNIT CELL GEOMETRIES

by

BENJAMIN GABRIEL MACKEY

A THESIS

Presented to the Graduate Faculty of the

MISSOURI UNIVERSITY OF SCIENCE AND TECHNOLOGY

In Partial Fulfillment of the Requirements for the Degree

MASTER OF SCIENCE

in

MECHANICAL ENGINEERING

2023

Approved by:

Dr. Kelly O. Homan, Advisor
Dr. Umit Koylu
Dr. Daniel Stutts

PUBLICATION THESIS OPTION

This thesis consists of the following two articles, formatted in the style used by the Missouri University of Science and Technology.

Paper I: Pages 6-34 are intended for submission to the International Journal of Heat and Mass Transfer.

Paper II: Pages 35-59 are intended for submission to the International Journal of Heat and Mass Transfer.

ABSTRACT

Honeycombs, metal foams, and lattice structures all provide a way to increase heat transfer due to better fluid mixing and larger surface area. Specifically, lattice structures can be a great way to provide heat transfer enhancement due to the ability to customize and optimize the unit cell geometry. In this research, a novel yet simple unit cell geometry is chosen for study. Four different configurations are tested in a lower Reynolds number range, 300–1800: single unit cell, two unit cells in series, three unit cells in series, and a 3x3 unit cell array. The Sherwood number of each configuration is found by using the naphthalene sublimation technique. Due to the parts being constructed using additive manufacturing, the partially localized Sherwood number can be found for each truss and also averaged over the area of the naphthalene-coated parts. The single unit cell configuration's overall performance is similar to the center unit cell's in the array; however, the wake is quite different behind each. The wake difference in the array is likely due to contribution of additional turbulence by the outside unit cells. The back unit cell on the two in series configuration has a slight reduction in performance compared to a single unit cell, and the back unit cell on the three unit cells in series has no noticeable reduction in performance compared to the back unit cell in the two in series configuration. When comparing the overall transfer to a cylinder in crossflow, the single unit cell, two unit cells in series, three unit cells in series, and array exhibit from 5% to over 40% higher Sherwood numbers, respectively.

ACKNOWLEDGMENTS

First and foremost, I would like to thank my advisor, Dr. Kelly O. Homan. Dr. Homan provided me with the tools and knowledge to begin my experimental work. It was also tremendously helpful Dr. Homan knew so much about Python, Linux, and LaTeX which provided me with tools to efficiently write my thesis. His classes also provided me with a greater proficiency in theoretical and computational fluids, which ultimately helped with my experimental work.

I would also like to thank my committee members, Dr. Koylu and Dr. Stutts, for their valuable time and advice in reviewing this thesis.

I would like to thank the people of my research group, Ajay Banala and Yi Qiao, for providing help when I needed it in my experimental work and in writing this thesis.

I am thankful for the funding and support provided by the Kansas City National Security campus.

Finally, I would like to thank my family and friends for supporting me in my pursuit of my master's degree.

TABLE OF CONTENTS

Page

SECTION

LIST OF ILLUSTRATIONS

PAPER II

SECTION

LIST OF TABLES

1. INTRODUCTION

There is always a need for improvements in heat transfer enhancement. Some relatively newer ways of providing enhancement include cellular materials. These cellular materials provide better fluid mixing and high surface area which leads to an increase in heat transfer. The more popular cellular materials include honeycomb structures which are regular patterns of tetragonal, pentagonal and hexagonal shapes, and metal foams, which are random patterns of various sized trusses [23]. A new cellular material has recently emerged due to advances in additive manufacturing (AM). These geometries are called lattice structures and they are comprised of repeated geometries called unit cells. AM allows the ability to customize the unit cell geometries for specific needs and also the ability to optimize the shape easily. Some unit cell geometries that have been studied include rhombi-octet, Kagome, x-type, pyramidal and tetrahedral [14].

This thesis contains two papers that experimentally study the mass transfer from different configurations of a simple but unique unit cell geometry using the naphthalene sublimation technique. In addition, the turbulence intensity behind each configuration in the 300–1800 Reynolds number range in an open wind tunnel is also measured. The chosen unit cell geometry is three mutually perpendicular cylinders. The combination of AM and the naphthalene sublimation technique allows for the study of the local transfer coefficient in the trusses and the overall area-average in the entire naphthalene coated unit cell. Paper I looks at the mass transfer off three unit cell configurations: a single unit cell, two unit cells in series, and then three unit cells in series. Both the two unit cells in series and three unit cells in series have the downstream unit cell coated with naphthalene. Paper II looks at the mass transfer off of a central unit cell in a 3x3 unit cell array with four total coated legs. Both Paper I and Paper II use hot wire anemometry to obtain the local streamwise mean velocity at various points downstream of the unit cell to calculate the turbulence intensity.

2. LITERATURE REVIEW

2.1. CELLULAR MATERIALS

Cellular materials are a popular way of providing enhanced heat transfer in various applications such as heat sinks, heat pipes and heat exchangers [23]. Some examples of these metal structures include metal foams which are made up of tortuous and random highly conductive metal struts, and lattice structures which are made up of repeated geometries called unit cells.

2.1.1. Metal Foams. Metal foams are a porous material usually comprised of randomly distributed struts that are made with a highly conductive metal such as aluminum or copper. These foams are attractive due to their ability to provide increased fluid mixing, large surface area, great mechanical strength, and high thermal conductivity if using special conductive metals [28]. Due to the popularity of these metal foams, there are a multitude of papers that have studied the properties. They produce a higher relative heat transfer, but at the cost of an undesirable higher pressure drop [2, 5, 7, 11, 12, 19, 20, 26, 28, 32].

2.1.2. Lattice Structures. Lattice structures unlike metal foams are much more customizable due to the randomness in metal foams from their manufacturing process. Kim et al. [16] performed an experimental study on lattice frame materials (LFM) using a sandwich style heat sink. The LFM style heat sink performed similarly to a conventional cylindrical tube array heat sink. However, in terms of efficiency, the LFM heat sink performed two times better compared to a bank of cylinders due to a lower flow resistance. When compared to an empty channel, the LFM removed six times as much heat compared to an empty channel due to a thermal dispersion effect created by an increased turbulent flow. In a new study, Kim et al. [17] numerically and experimentally researched an LFM with tetrahedral type unit cells. It was observed that the dominant flow features include vortex structures behind the vertices of the unit cell and flow separation at the strut surface.

One of the two types of vortices include a horseshoe shape which forms in front of the vertices of the unit cell. The other is an arch-shaped vortex which forms behind the vertices. The horseshoe vortices increased heat transfer by up to 180% at the endwall compared to areas that don't have those vortices present, and the arch vortices increased heat transfer by introducing recirculating and reattachment. Areas with flow separation produced 40% of the total heat transfer. Comparing the performance of the tetrahedral LFM to other heat transfer media such as packed beds and empty channels in terms of thermal efficiency, the LFM performs better.

Another unit cell topology is Kagome. Shen et al. [25] researched the effect of replacing pin fin arrays with Kagome unit cells. The model with three arrays of Kagome lattices performed 9–28% and 16–71% better than two arrays and three arrays of pin fins, respectively at a fixed porosity and in the 5000–25000 Reynolds number range. Although the three arrays of Kagome unit cells had superior thermal performance compared to the other pin fin configuration, the pressure drop across all of them is the same. Xu et al. [29] looked at customizing the Kagome unit cell to optimize the topology. It was found increasing the truss diameter and inlet Reynolds number increased the overall heat transfer. More specifically, increasing the ratio of column diameter to channel height increases the Nusselt number of the channel wall. Increasing the inclination angle and included angle in the Kagome geometry lowered the Nusselt number. This shows there are ways to optimize a certain unit cell geometry by changing several different parameters.

Bai and Chung [2] introduced a new topology called the windward bend structure in addition to comparing the performance of other cellular materials including metal foams, corrugated structures and lattice structures with pyramidal, Kagome, and tetrahedral unit cell topologies. In this study, the metal foams provide higher heat transfer but at an increased pressure drop; however, at any given pumping power, the Nusselt number is lower. Their own geometry, the windward bend structure, had 1.2–1.3 times higher Nusselt number

compared to corrugated structures and the lattice core structures with Kagome, pyramidal, and tetrahedral unit cells at a given pumping power. This larger Nusselt number is believed to be caused by macroscopic thermal dispersion.

Yan et al. [30] studied x-type units and compared their performance to LFM and Kagome geometries. At a fixed porosity, the x-type unit cells obtained 170% increase in heat transfer when compared to than an LFM and 100% better heat transfer than a Kagome geometry. This is most likely due to the spiral primary flow, and two cross flows and a vortex pair in the secondary flows. The primary flows led to a 90% higher overall Nusselt number, and the secondary flows led to a 20% overall increase in Nusselt number on the end walls. Even at a fixed pumping power, the x-type performs better than both geometries. Yan et al. [31] then moved to testing these x-type unit cells in brake discs. The brake discs with the x-type unit cells obtained 18–21% higher overall Nusselt number compared to a radial vane brake disc within the operating range of a passenger vehicle. Xi et al. [27] tried to optimize the shape of the x-type unit topology. Both increasing the inlet Reynolds number, the ratio of truss diameter to channel height, increased the Nusselt number. Increasing the ratio of transverse spacing to characteristic length decreased Nusselt number, and increasing the ratio of streamwise spacing to characteristic length, increased then decreased the Nusselt number.

AM has allowed for more complex shapes to be printed and experimentally tested. Ho et al. [10] designed a rhombi-octet unit cell and used selective laser melting to construct two differently sized lattice heat exchanger. The larger lattice contained 7 mm sized unit cells and the larger one included 14 mm sized unit cells. The 7 mm lattice obtained a 40–45% higher thermal conductance compared to the 14 mm lattice, and both lattice heat exchangers had up to two times larger heat transfer coefficient compared to a traditional fin-tube heat exchanger. Another complex topology, the octet-truss unit cell, was tested by Chaudhari et al. [6]. An AM process called direct metal laser sintering was used to construct the unit cell out of an aluminum alloy. The objective of this experiment was

to test the porosity effect on heat transfer. The lattices with 70.6% and 86.9% porosities performed similar in terms of Nusselt number and the 91.3% porosity lattice performed worse. Broughton and Joshi [4] designed a rhombic dodecahedron lattice and constructed it using direct laser sintering. They wanted to compare their geometry to a traditional metal foam. The 60% increase in heat transfer in the rhombic dodecahedron lattice compared to the metal foam also resulted in a 60% increase in pressure drop. Despite this, the lattice exhibited a better overall thermal performance as a function of pumping power. AM allowed Liang et al. [18] to experimentally test four types of unit cells including x-type, Kagome, face centered cubic (FCC) and body centered cubic (BCC) by printing them with selective laser melting. If comparing the overall thermal efficiencies, the BCC lattice performed the best with the x-type, pin fin, and Kagome coming in second, and the FCC performing the worst.

2.2. NAPHTHALENE SUBLIMATION TECHNIQUE

The naphthalene sublimation technique is a way to find the mass transfer and therefore heat transfer off a geometry that can be coated. This method can find the area average transfer by measuring the change in mass of naphthalene or locally by measuring the change in depth of the naphthalene surface. The methodology of the technique is as follows:

1. Mold or coat the geometry with naphthalene.
2. Before the testing, weigh the specimen if finding the area average transfer or measure the surface profile if finding the local transfer.
3. Run the desired experiment with naphthalene coated geometry.
4. Weigh or measure the surface profile again.

Once the before and after measurements are obtained, the data can be reduced in combination with naphthalene properties to obtain the Sherwood number and eventually the Nusselt number using the heat and mass transfer analogy [9].

PAPER

I. AREA AVERAGE SURFACE TRANSFER COEFFICIENTS IN UNIT CELLS IN SERIES

Benjamin Mackey & K. O. Homan
Department of Mechanical & Aerospace Engineering
Missouri University of Science and Technology
Rolla, Missouri 65409–0050
Tel: 573–341–6622, Fax: 573–341–4115
Email: khoman@mst.edu

ABSTRACT

Lattice structures, which are made up of repeated patterns of a geometry called unit cells, provide a way to increase surface transfer. In this study, a unique geometry is chosen for the base unit cell. The surface transport is found experimentally using the naphthalene sublimation technique and the wake is examined using hot wire anemometry in a Reynolds number range of 300–1800 in 300 Reynolds number intervals. Three different configurations are studied: a single unit cell, two unit cells in series, and three unit cells in series. A localized transport coefficient is found for the individual trusses that make up the unit cell by using additive manufacturing to aid in the molding of the naphthalene coated pieces. The overall transport is found by averaging the total mass transfer over the combined trusses over the entire naphthalene coated area. All trusses, regardless of the orientation in the wind tunnel, are individually compared to the Churchill-Bernstein Sherwood number correlation for cylinders in crossflow. Over the interval, the unit cell configurations perform better than a cylinder in crossflow. The single unit cell has a 16–42% increased transfer. The back unit cell on two unit cells in series has a 12–29% better transfer than a cylinder, and

the back unit cell on three unit cells in series has a 16–29% better transfer than a cylinder at. There is also little reduction in performance when comparing the single unit cell to the back unit cell on the series configurations. These unit cell geometries provide better mass transfer and therefore an expected improvement in heat transfer in the in the lower Reynolds number range and get increasingly better transfer as the Reynolds number increases.
Keywords: forced convection, naphthalene sublimation, unit cells in series, lattices, mass transfer, hot wire anemometry

1. INTRODUCTION

Heat transfer enhancement is consistently improved upon due to the importance in many engineering applications. There is a need for more compact and efficient ways of providing enhancement. Current technologies involve using cellular materials such as porous materials or lattice structures due to their high surface area and ability to provide better fluid mixing and turbulence. A popular porous material includes open-cell metal foams that are usually made of a highly conductive metal like aluminum or copper and consist of struts and interconnected pores that are tortuous and randomly distributed. The metal foams are desired due to their low density, large surface area, an ability to provide better fluid mixing, high thermal conductivity, and high strength [1] Several studies have been completed computationally [2–4], analytically [1, 5–8] and experimentally [9, 10] that demonstrate an increased heat transfer performance although at the expense of an undesirable higher pressure drop. Open cell metal foams can be used in a variety of applications including compact heat exchangers, heat sinks and even in industries that require the mechanical properties of the foams including transportation, aerospace, biomedical, and construction [11, 12].

More recently, lattice structures have been studied due to their ability to provide outstanding mechanical properties, enhanced heat transfer and due to advances in additive manufacturing, the potential to be customized for different applications. Sajjad et al.

[13] and Kaur and Singh [14] provide comprehensive studies of papers involving different types of unit cell geometries in lattices. Lattice structures are a repeated pattern of a geometry called a unit cell and these unit cells are normally composed of cylindrical struts in various topologies including tetrahedral, Kagome, pyramidal and X-type structures. Unlike traditional metal foams, these lattices are uniform, can be highly customized due to the flexibility of additive manufacturing, and can provide a favorable pressure drop.

An early experimental study on lattice frame materials (LFM) was completed by Kim et al. [15] using an LFM sandwich style heat sink. In heat removal, both LFM topologies performed similarly to a convectional cylindrical tube array in a heat sink but in efficiency, one of their LFMs performed about twice as high compared to their other LFM geometry and a bank of cylinders due to the lower flow resistance. It was observed that the LFM creates a greater turbulent flow and results in a thermal dispersion effect which removed six times more heat compared to an empty channel. Then Kim et al. [16] moved on to a numerical and experimental study on how the local fluid flow behavior affects pressure drop and heat transfer of an LFM with a tetrahedral unit cell. The dominant flow features consist of vortex structures behind the vertices of the LFM and flow separation at the strut surface. The horseshoe-shaped and the arch-shaped vortex structures form in front of and behind the vertices of of the unit cell, respectively. The horseshoe vortices at the endwall improved local heat transfer up to 180% when compared to regions where the horseshoe vortices are barely active. The arch-shaped vortices improve heat transfer due to the flow recirculation and reattachment. 40% of the total heat transfer comes from the strut surface before flow separation. The performance of the LFM was compared to other heat transfer media at a fixed pumping power and it revealed that LFMs are a better heat transfer media than packed beds and an empty channel with a superior thermal efficiency, ($Nu/f^{1/3}$), to most other heat transfer media.

A specific type of unit cell topology, Kagome, was investigated by Shen et al. [17] by replacing pin fins with the Kagome structure. For a fixed porosity and Re in the 5000–25000 range, the three Kagome lattice array model's overall Nusselt is 9–28%, 6–25%, and 16–71% higher compared to models with two arrays of pin fins, two arrays of Kagome lattices, and three arrays of pin fins, respectively. The two arrays of pin fins and two arrays of Kagome lattices have similar thermal performance. As $y < 0.1m$, the average temperatures and Nusselt numbers are similar for each model. The inner region's Nusselt numbers of the three Kagome lattice array are 75% higher compared to the two arrays of pin fins and two arrays of two Kagome lattice array models and 44% higher than the two Kagome lattice array model downstream. From $0.1m < y < 0.19m$, the three Kagome lattice array model's sidewall has 20–309% better cooling compared to other models due to reduction of recirculation at the tips. The three Kagome array model's tip has a small recirculation region due to "shunting" effect of the Kagome lattices which forces high velocities at the tip and improves the thermal performance. Under the same Reynolds number and porosity, all the models produced the same pressure drop. Xu et al. [18] looked at changing the geometric parameters of the Kagome unit cell. It was found that increasing the ratio of column diameter to channel height from 0.1 to 0.2 improved the heat transfer significantly, increased the friction factor by 60.9% and increased the Nusselt number of the channel wall by 32.2%. On the other hand, when the inclination of the column increased from 45° to 60°, the friction factor is decreased by 22.8% and the Nusselt number decreased by 13.2%. When the included angle of the column is increased from 120° to 150°, the friction factor decreases by 28.5% and the Nusselt number decreases by 13.9%. The geometric parameters of a certain unit cell topology can have a profound impact on the overall heat transfer.

Yan et al. [19] looks at forced convection over an x-type lattice structure and compares the results to other periodic cellular materials including tetrahedral (LFM) and Kagome. The x-type lattices performed up to 100% and 170% better than LFM and Kagome lattices respectively in heat transfer enhancement. The overall enhancement in the x-type

lattices is proposed to be caused by a spiral primary flow and three different types of secondary flows: two cross flows and one vortex pair. These flows induce a 90% and 20% higher area-averaged Nusselt numbers on the end wall and cell ligaments respectively when compared to the LFM. The x-type lattice has a higher heat transfer and thermal efficiency at a fixed pumping power but at a 3.2 and 3.6 times higher pressure drop compared to the tetrahedral and Kagome structures, respectively. Bai and Chung [4] performed numerical simulations of forced convection over sandwich panels filled with metal foam, corrugated cellular structures and lattice core structures including Kagome, tetrahedral, and pyramidal and introduced their own topology named the windward bend structure. The metal foam provides higher heat transfer but at a higher pressure drop at the velocity so at a given pumping power, the Nusselt number is lower compared to lattice core structures. The windward bend's Nusselt number, over the same pumping range power, is 1.2 to 1.3 times greater than the corrugated cellular and lattice core structures. It is believed this superior heat transfer efficiency is due to its better macroscopic thermal dispersion.

Due to recent advances in additive manufacturing (AM), new cellular structures can easily be fabricated, and previous cellular structures can be easily manipulated. Ho et al. [20] used selective laser melting to fabricate two lattice heat exchangers out of an aluminum alloy. AM allowed them to design their lattice with a complex topology called Rhombi-Octet unit cell which has a higher packing density and lower porosity than aluminum foams. The Rhombi-Octet lattices have a two times greater heat transfer coefficient than a a fin-tube heat exchanger at the same mass flow rate and a 45% higher heat transfer coefficient than a fin-tube heat exchanger at the same pumping power to depth of heat exchanger ratio. Chaudhari et al. [21] used another form of AM called direct metal laser sintering to design an octet-truss unit cell geometry out of an aluminum alloy and experimented with different lattice porosities. The 70.6% and 86.9% porosity lattices produced similar Nusselt numbers (based on hydraulic diameter) at the same Reynolds numbers and the 91.3% porosity lattice gave a smaller Nusselt number at the same Reynolds numbers. The pressure drop, when

compared to stochastic metal foams, was lower. Broughton and Joshi [22] also looked at experimental and computational comparisons between AM rhombic dodecahedron lattices and metal foams in single phase convection. In this case, the designed unit cell had a 66% higher pressure drop due to its rhombic shape but also a 60% increase in heat transfer. Even though the pressure drop is higher, the thermal performance as a function of pumping power of the AM unit cell is vastly superior to the metal foam.

As seen in the literature above, customized unit cells are a notable way to provide heat transfer enhancement. This paper aims to examine the surface transfer coefficients of a unique, but relatively basic unit cell geometry in forced convection. This specific unit cell geometry is a piece that can be further customized and be used in a repeated pattern lattice structure. The combination of AM and the naphthalene sublimation technique allows the experimental study of the local transfer coefficients of each truss in a single unit cell and in the downstream unit cell in a series of unit cells. Unlike most studies, this paper aims to experimentally study the surface transfer coefficients of the specifically designed unit in an open wind tunnel, not attached to any sandwich panels, and to study the individual truss performance at lower Reynolds numbers. The main objective of this paper is to obtain the Sherwood number of the various trusses and the area average over the entire studied unit cell in different configurations including a single unit cell, two unit cells in series, and three unit cells in series. The second objective is to look at the flow behind the three different configurations at two different planes at various locations downstream using hot wire anemometry. Overall, the goal is to determine how the subsequent unit cells in series and their trusses perform in relation to other unit cells in a series.

2. METHODS AND APPARATUS

2.1. NAPHTHALENE SUBLIMATION TECHNIQUE

The basic unit cell is comprised of three mutually perpendicular cylinders. The unit cells in this experiment consist of three cylinders with an L/D = 6. The diameter of the cylinders is 5/8 inch and as a result of the L/D restriction, the length is 3.75 inches. Three different configurations are chosen for this experiment: a single unit cell (Figure 1a), two unit cells in series (Figure 1b), and three unit cells in series (Figure 1c). The single unit cell is designed with five total cylindrical trusses and the two and three unit cells in series feature four detachable trusses. The detachable trusses include a 1/4 in. recess (Figure 3a) to mold the naphthalene to the surface of the truss and are attached to the unit cell via a metal dowel pin shown in Figure 1a. A stand is designed to prevent the unit cell configurations from rotating and to keep it balanced in the center of the wind tunnel (diagram show in Figure 2). The unit cell and their parts are printed using an AM technique called selective laser sintering (SLS) with nylon 12.

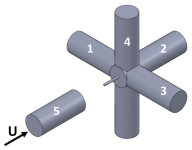

(a) Single unit cell with detachable trusses.

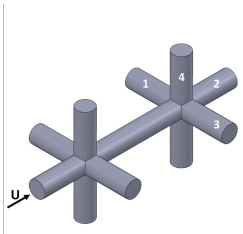

(b) Two unit cells in series .

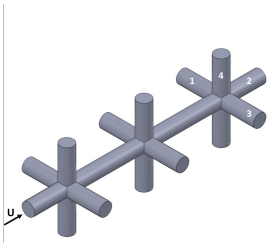

(c) Three unit cells in series.

Figure 1. Unit cell configurations.

Once the design of the unit cell is completed, a mold is needed to attach the naphthalene to the detachable unit cell trusses. The first iteration of the aluminum mold included one pour hole for each respective truss for a total of four trusses. The second iteration of the aluminum mold included a pour hole and two runners for each respective

truss for a total of five trusses. This allowed for a smoother molding process and a higher success rate. Each of the molds are machined with a smooth inside surface so the surface of the naphthalene could be as smooth as possible. The final mold design cross section is shown in Figure 3b.

(a) A single detachable truss with naphthalene recess.

(b) Cross section of mold.

Figure 3. Molding parts.

The first part of the molding process involves melting down moth balls with a purity of 99.95% naphthalene using a IKA C-MAG HS 7 hot plate. The hot plate is set to 450 degrees C. Once the naphthalene reaches its boiling point, it is taken off of the hot plate and allowed to settle for 30 seconds to stop the boiling. The molten naphthalene is poured into the mold and allowed to sit for about an hour to allow the molten naphthalene to reach room temperature. To get the multiple trusses out of the mold, one half of the mold is hit with a hammer to create a shearing force on the naphthalene surface (recommended by Goldstein and Cho [23]). The runners are carefully cut off to achieve an adequate

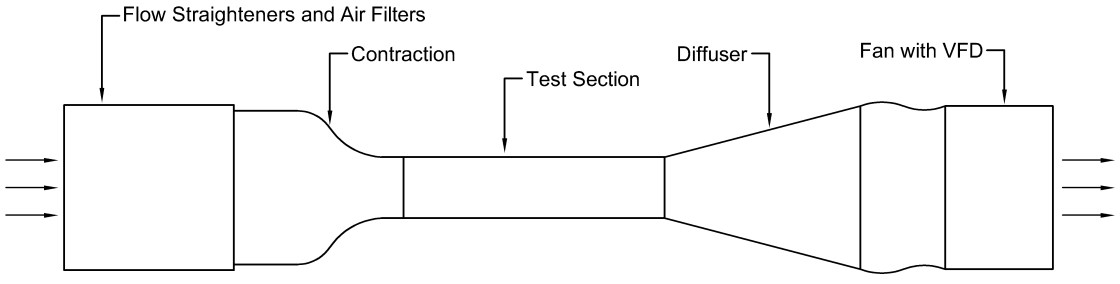

Figure 2. Wind tunnel setup.

cylinder surface profile. The trusses are inspected for surface defects and if they pass the inspection, the trusses are immediately placed in a plastic bag with a few moth balls to slow the sublimation process and preserve the cylindrical naphthalene surface. To minimize naphthalene surface temperature change, the naphthalene trusses in the bag are allowed to reach room temperature again before testing to ensure a constant temperature of the naphthalene surface throughout the whole test. Both the surface temperature and the mass of the trusses are measured separately before attaching them and putting the unit cell in the wind tunnel. The temperature was taken using a type k thermocouple wired to an OMEGA HH82 digital thermometer which can read the temperature to an accuracy of 0.1 degrees C. The mass of each naphthalene truss is measured using a Sartorius BP211D with an accuracy of 0.01 mg. They are then attached to the unit cell configuration and set in the wind tunnel running at the desired velocity. The unit cell configuration is taken out of the wind tunnel, the trusses are disconnected from the unit cell and then the trusses' surface temperature and mass are taken again. The experimental test matrix for each unit cell configuration is shown in Table 1.

Table 1. Unit cell tests (U_∞ in m/s, Δm in mg, τ in minutes, T in $^\circ C$).

	Single Unit Cell (5 trusses)				Two Unit Cells in Series (4 trusses)				Three Unit Cells in Series (4 trusses)			
Re_{nom}	U_∞	Δm	τ	T	U_∞	Δm	τ	T	U_∞	Δm	τ	T
300	0.29	94.90	90.0	20.9	0.28	84.12	91.6	20.6	0.28	56.82	63.0	20.2
	0.29	50.89	45.1	20.4	0.28	42.57	45.6	20.6	0.28	40.65	45.2	20.0
600	0.57	147.11	90.1	20.6	0.57	126.56	89.8	21.1	0.57	60.57	45.2	20.4
	0.57	74.06	45.1	20.3	0.57	64.09	45.2	20.8	0.57	49.81	36.6	20.1
900	0.87	137.76	60.0	20.4	0.86	101.61	61.2	20.8	0.87	68.76	40.2	20.6
	0.87	67.12	31.0	20.1	0.86	51.00	29.9	20.1	0.87	53.62	30.3	20.5
1200	1.14	116.66	45.7	20.0	1.14	95.07	46.0	20.7	1.15	80.87	40.2	20.3
	1.14	75.94	30.0	19.9	1.14	64.14	30.0	20.6	1.15	62.02	30.1	20.4
1500	1.43	76.31	25.5	20.1	1.44	77.53	30.1	20.4	1.45	98.69	41.7	20.5
	1.43	73.99	25.4	19.9	1.44	96.82	40.5	20.3	1.45	67.63	30.3	20.1
1800	1.73	82.11	25.5	19.9	1.73	79.30	30.2	20.8	1.73	99.56	40.4	20.3
	1.73	77.65	25.2	19.5	1.73	94.68	35.2	20.4	1.73	79.22	30.5	20.1

2.2. AREA AVERAGE MASS TRANSFER COEFFICIENT CALCULATION

The area average transfer coefficient involves taking the change in the mass of the naphthalene cylinder over time and is represented by

$$\dot{m} = \frac{m_b - m_a}{\tau} \tag{1}$$

where m_b is mass of the naphthalene cylinder before the sublimation in the wind tunnel and m_a is the mass after sublimation. The mass transfer coefficient is given by

$$h_m = \frac{\dot{m}}{A_s(\rho_{v,w} - \rho_{v,\infty})} \tag{2}$$

where A_s is the surface area of the naphthalene given by $A_s = \pi DL$, $\rho_{v,w}$ is the vapor density of the naphthalene at the surface and $\rho_{v,\infty}$ is the vapor density of naphthalene in the freestream. It is assumed the density of the naphthalene in the freestream is negligible ($\rho_{v,\infty} = 0$) since the lab has significant ventilation to clear the air of any naphthalene vapor. The vapor density of the naphthalene at the surface is calculated using the ideal gas law given by

$$\rho_v = \frac{P_v}{R_{nap}T} \tag{3}$$

where R_{nap} is the individual gas constant for naphthalene ($R_{nap} = 64.871 J/kgK$) and is found by dividing the universal gas constant ($R_u = 8.3145 kJ/kmolK$) by the molar mass of naphthalene (128.17 kg/kmol). The temperature of the naphthalene surface is denoted by T and P_v is the naphthalene vapor pressure. The naphthalene vapor pressure is calculated using the correlation found by Ambrose et al. [24],

$$TlogP_v = \frac{1}{2}a_0 + \sum a_n E_n(x) \tag{4}$$

$$x = \frac{2T - 574}{114} \tag{5}$$

where $a_0 = 301.6247$, $a_1 = 791.4937$, $a_2 = -8.2536$, $a_3 = 0.4043$, $E_1(x) = x$, $E_2(x) = 2x^2 - 1$, and $E_3(x) = 4x^3 - 3x$. Then the Sherwood number, based on the characteristic length of the of the naphthalene trusses (in this experiment, depending on the orientation of the truss, $L_c = L$ or $L_c = D$) $L_c = L$ or $L_c = D$, can be calculated,

$$Sh = \frac{h_m L_c}{D_f} \tag{6}$$

The diffusion coefficient of naphthalene in air, D_f, is calculated using the correlation given by Goldstein and Cho [23],

$$D_f = 0.0681 \left(\frac{T}{298.1}\right)^{1.93} \frac{1.013 \times 10^5}{P} \tag{7}$$

Once the Sherwood number is found, then the Nusselt number can be calculated from the heat and mass transfer analogy,

$$Nu = Sh \left(\frac{Pr}{Sc}\right)^n \tag{8}$$

where n can range from 1/3 to 0.4 [23] and is found from empirical results. To implement the analogy, the Schmidt number and Prandtl numbers need to be equal. In this experiment, the Schmidt number is 2.23 for naphthalene in air and the Prandtl number is 0.71 for air, but according to Goldstein and Cho [23] it can still be and has been applied with assurance. The Schmidt number can also be found more accurately by the Keumnam et al. [25] correlation,

$$Sc = 8.0743 T^{-0.2165} \tag{9}$$

2.3. HOT WIRE ANEMOMETRY

To complement the measured mass transport, a Dantec Dynamics single wire anemometer is utilized to measure the locally, unsteady velocity in the wind tunnel and unit cell wake. The hot wire is attached to a Dantec Systems Multichannel CTA 54N82. StreamWare Basic software is used to calibrate the hot wire and record velocity and time data. Solid unit cell configurations (without detachable trusses and naphthalene recesses) are printed to avoid possible unwanted interactions. The hot wire measurements are taken at four locations downstream of the unit cell at $x/d = 0$, $x/d = 3.0$, $x/d = 6.6$, and $x/d = 9.6$ which is shown in Figure 4a. The x-locations are limited due to the wind tunnel setup. Fourteen hot wire data points are taken along each of those x-locations except for at $x/D = 0$ due to truss 4 blocking the ability to take data points in that location. That plane of points is used to take data at two different y-locations, $y/D = 0.5$ and $y/D = 1.5$ which is shown in Figure 4b. These data points are used to make a contour plot of the average velocity and turbulence intensity and due to the nature of the formation of the contour plots, there is some interpolation happening between the points.

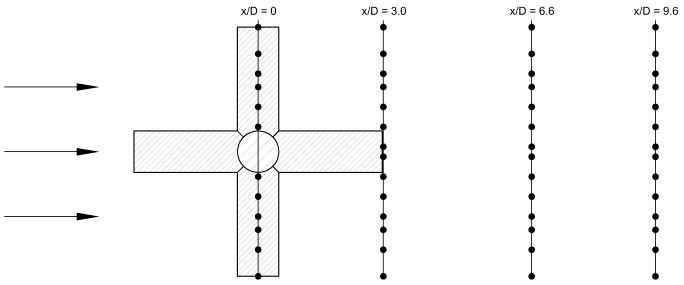

(a) Top view.

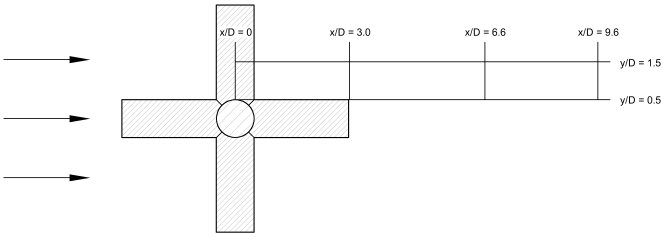

(b) Side view.

Figure 4. The different planes and data points taken using the hot wire anemometer.

2.4. VALIDATION OF THE NAPHTHALENE SUBLIMATION TECHNIQUE

Since circular cylinders are a well-researched geometry, they were tested to validate our implementation of the naphthalene sublimation technique. The cylinders are printed using the same SLS method as the unit cell geometries and incorporate a similar naphthalene recess. The diameter of the cylinder is 5/8 in. The cylinders utilize a square hole to attach to square mounts on a printed frame to prevent any rotation during testing. The cylinders were tested over a range of Reynolds numbers as shown in Table 2. The results of the naphthalene cylinders tests are show in Figure 5 with an average uncertainty of around 10.2% and compared with the Churchill-Bernstein correlations for circular cylinders in forced convection [26],

$$\overline{Nu} = 0.3 + \frac{0.62Re^{1/2}Pr^{1/3}}{\left[1 + (0.4/Pr)^{2/3}\right]^{1/4}} \left[1 + \left(\frac{Re}{282000}\right)^{5/8}\right]^{4/5} \tag{10}$$

Using the heat and mass transfer analogy, the Churchill-Bernstein correlation can be used to find the area average Sherwood number by replacing the Prandtl with the Schmidt number so the equation becomes

$$\overline{Sh} = 0.3 + \frac{0.62Re^{1/2}Sc^{1/3}}{\left[1 + (0.4/Sc)^{2/3}\right]^{1/4}} \left[1 + \left(\frac{Re}{282000}\right)^{5/8}\right]^{4/5} \tag{11}$$

There is greater error towards the lower Reynolds number range and Churchill and Bernstein [26] mentions Nu_0 (0.3 at the beginning of the equation) value or in this case the Sh_0 value is arbitrary and can be modified for any given data set. The chosen value for Sh_0 for this experimental data is 2.1 which gives a better fit. The larger error in the lower Reynolds number range could also be attributed to the wide range of experimental conditions under which this equation was derived.

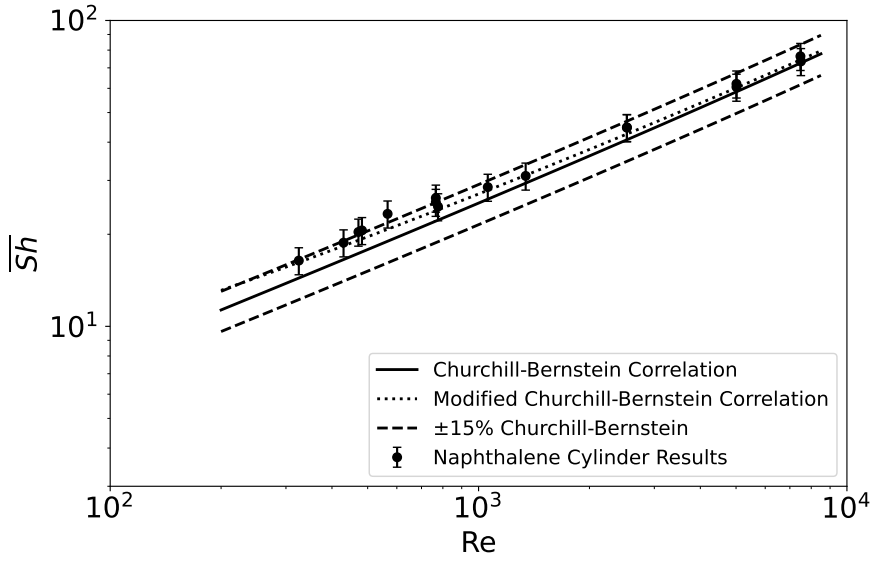

Figure 5. Comparison of naphthalene sublimation Sherwood number results to the Churchill and Bernstein [26] correlation.

Table 2. Circular cylinder tests (Δm in mg, τ in minutes, T in $^{\circ}C$).

Re	Δm	τ	T
330	110.41	90.2	21.0
430	44.92	32.1	21.0
470	175.02	121.4	20.9
480	175.35	120.2	20.8
570	177.27	120.4	20.4
760	342.27	180.0	21.4
760	160.55	85.4	21.4
780	310.65	187.6	20.8
1060	150.96	74.7	21.0
1340	99.18	45.1	21.0
2520	105.43	37.0	20.2
2520	108.95	38.3	20.2
5010	124.50	30.8	20.1
5010	129.12	32.4	20.2
7470	153.7	33.6	19.9
7490	172.3	33.5	21.0

3. RESULTS AND DISCUSSION

3.1. SINGLE UNIT CELL

To understand the experimental Sherwood number values, the flow past the unit cell and the flow past a cylinder are compared. The hot wire data is taken and converted to turbulence intensity contours. The flow past a cylinder at $Re = 300$ and $Re = 1800$ is shown in Figure 6a and Figure 6b, respectively. The cylinder produces a symmetrical wake at both Reynolds numbers and due to the smaller average streamwise velocities and larger fluctuations, the wake behind the cylinder at $Re = 300$ has higher turbulence intensities.

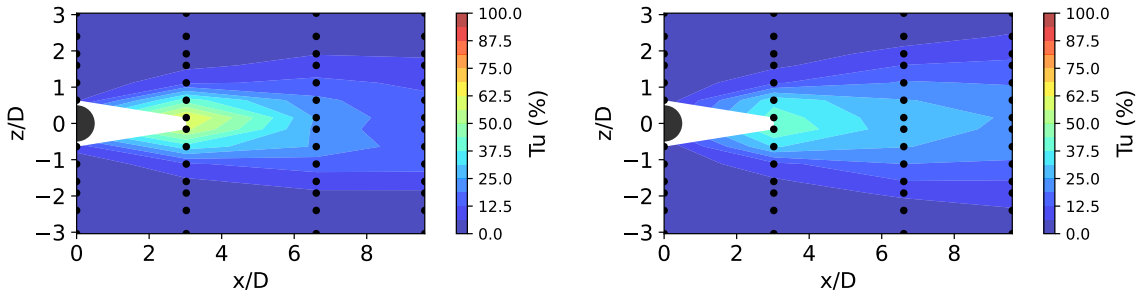

(a) Re = 300. (b) Re = 1800.

Figure 6. Turbulence intensity downstream of a single circular cylinder.

The flow downstream of single unit cell at $y/D = 1.5$ and at $y/D = 0.5$ is shown in Figure 7 and Figure 8, respectively. The wake behind the single unit cell at $Re = 300$ (Figure 7a) is quite different when compared to the equivalent cylinder flow (Figure 6a). The unit cell produces two different smaller symmetrical turbulent regions at a higher turbulence intensity but smaller overall combined wake. The maximum turbulence intensity downstream of the unit cell reaches around 155% due to the small average velocity and high deviation whereas the cylinder reaches maximum turbulence at around 65%. At $Re = 1800$ (Figure 7b), the wakes are somewhat similarly sized and symmetrical, but the wake behind the unit cell is slightly more turbulent compared to the cylinder. The maximum turbulence behind the unit cell and the cylinder is around 49% and 43%, respectively. The higher

turbulent region behind the unit cell is also larger in the area closer to the geometry. The wakes for the single unit cell at different Reynolds numbers display an apparent difference. $Re = 300$ produced two noticeably different turbulent regions whereas $Re = 1800$ produced one larger turbulent region; however, the split turbulence regions at $Re = 300$ are just noticeable downstream at $Re = 1800$ in the range of $6 < x/D < 9.6$ due to a possible transition between the Reynolds numbers.

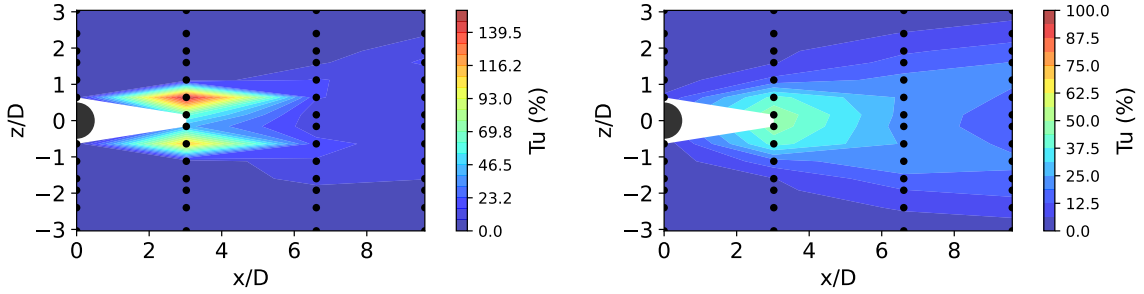

(a) Re = 300. (b) Re = 1800.

Figure 7. Turbulence intensity downstream a single unit cell at y/D = 1.5 at different Reynolds numbers.

The more pronounced differences are observed at $y/D = 0.5$ (Figure 8) which is right above the where all the trusses meet. At $Re = 300$ (Figure 8a), the flow seems to separate into four different even smaller turbulence zones. The zones in the positive z/D are slightly larger than the zones in the negative z/D positions with larger turbulence intensities as well. There also seems to be correlation to the turbulent zones at $y/D = 1.5$ with the turbulent zones around $z/D = -1$ and $z/D = 1$ at $y/D = 0.5$. The shedding from trusses 1 and 3 are contributing to the separate turbulent zones at plane $y/D = 0.5$ since those other two zones at $z/D = -1.5$ and $z/D = 2.5$ are not present in Figure 7a. At $Re = 1800$, the overall turbulent zone is much larger due to the shedding off trusses 1 and 3. The zone is overall more uniform in the $-2 < z/D < 2$ range when compared to $Re = 300$ with higher turbulence intensities where the separate zones appeared in Figure 7a.

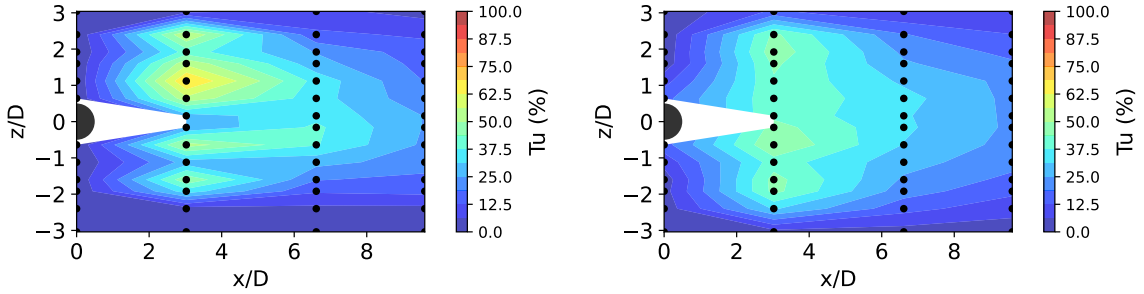

(a) Re = 300. (b) Re = 1800.

Figure 8. Turbulence intensity downstream of single unit cell at y/D = 0.5 at different Reynolds numbers.

The single unit cell has a total of five total naphthalene coated trusses. The Sherwood numbers for each truss based on the diameter of the truss are shown in Figure 9a. Trusses 1, 3, and 4 perform similarly at each tested Reynolds number with some variation in the trusses, and if averaging the trials, get 27–55%, 28–43%, and 28–44%, respectively better transfer compared to a cylinder (using the Churchill-Bernstein cylinder in crossflow correlation). If comparing the mixing behind each, the unit cell is getting better mixing and higher turbulence where the truss should be acting similarly to a cylinder at $y/D = 1.5$. This is most likely due to truss 5 introducing turbulence before the freestream flow reaches trusses 1, 3, and 5. Closer to where the trusses meet at $y/D = 0.5$, at $Re = 300$, there are highly turbulent multiple mixing zones and at $Re = 1800$, there is a larger more turbulent region causing a higher transfer off the lower part of the trusses. The Sherwood number for trusses 2 and 5 are consistently lower when compared to the other three trusses if using the diameter as the characteristic length, and truss 2 consistently performs better than truss 5 most likely due to the increased turbulence and mixing slightly above and near it which is shown in Figure 8. Despite the orientation with respect to the freestream, trusses 2 and 5 on average begin to get 18–33% and 5–11%, respectively better transfer than a cylinder in crossflow at $Re = 900$. The uncertainty of each Sherwood number for all unit cell configurations is around 5.9%.

A flat plate correlation was used to compare to trusses 2 and 5 due to their orientation inside the wind tunnel. The start of the cylindrical "flat plate" is the point where the flow first collides with the blunt end of truss 5 and each truss 2 downstream is treated as a continuation of the flat plate. Two different correlations are used, laminar and turbulent, to get a better understanding of how they compare [27]:

$$\overline{Sh_L} = 0.664 Re_L^{1/2} Sc^{1/3}, \qquad \text{Laminar} \tag{12}$$

$$\overline{Sh_L} = 0.0592 Re_L^{4/5} Sc^{1/3}, \qquad \text{Turbulent} \tag{13}$$

where L represents the length of the combined cylinders downstream depending on the unit cell configuration. Both trusses perform better than the turbulent flat plate at each point and only at one point at the lower end of the Reynolds number range does the laminar flat plate perform better than truss 5. Trusses 5 and 2 get 30-64% and 73-109% better transfer than a turbulent flat plate, respectively. The experimental data, although larger, increases at the same rate as the turbulent flat plate correlation.

3.2. TWO UNIT CELLS IN SERIES

Due to the unsteady approach flow produced by the single unit cell, the wake behind two unit cells in series is expected to be different. Unlike the single unit cell, the two unit cells in series produce an asymmetric wake at $Re = 300$. The overall turbulence intensity in the wake of two unit cells in series decreases when compared to the single unit cell in the plane, $y/D = 1.5$ but the approaching flow is much more turbulent due to the turbulence produced by the upstream unit cell. The maximum turbulence in the wake is around 26% compared to the single unit cell's 155% turbulence intensity. This is also the case for $Re = 1800$; where the wake is less turbulent compared to the single unit cell under the same conditions, but the approaching flow is more turbulent. The maximum turbulence is

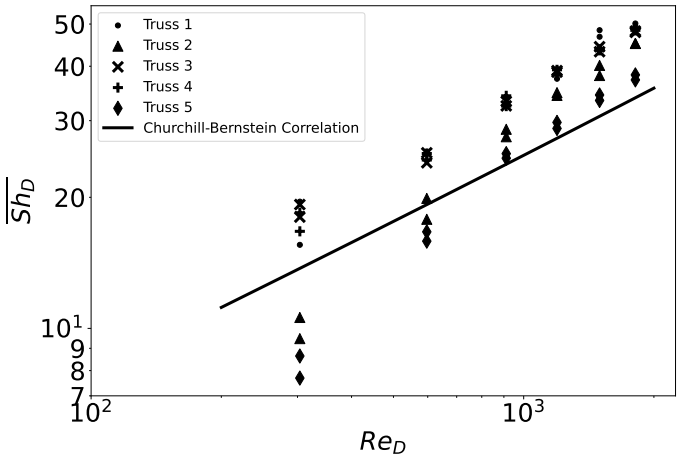

(a) Sherwood number based on the diameter for trusses 1, 2, 3, 4, and 5.

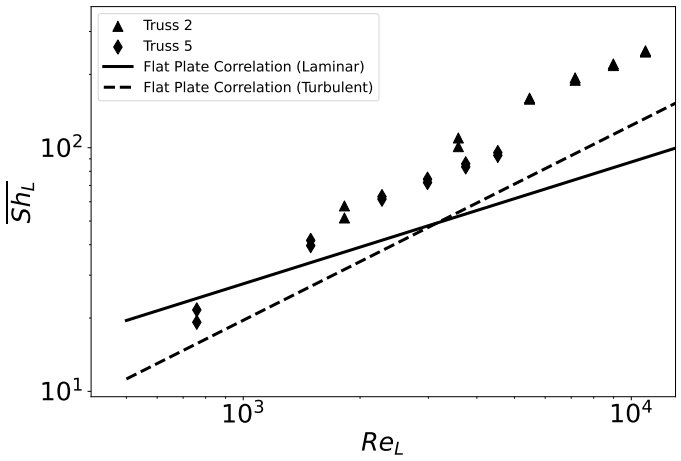

(b) Sherwood number based on the distance downstream relative to truss 5 upstream.

Figure 9. Sherwood number for the various naphthalene-coated trusses of the single unit cell.

around 35% compared to the 49% for the single unit cell. The turbulent approaching flow can be seen in at $x/D = 0$ at both Reynolds numbers in Figure 10. The turbulence extends out to both end points on the z/D axis at $Re = 1800$; however, it only extends to around $z/D = -1.75$ but does extend all the way to the positive z/D at $Re = 300$. From $Re = 300$ to $Re = 1800$, the flow transitions to create a symmetrical wake.

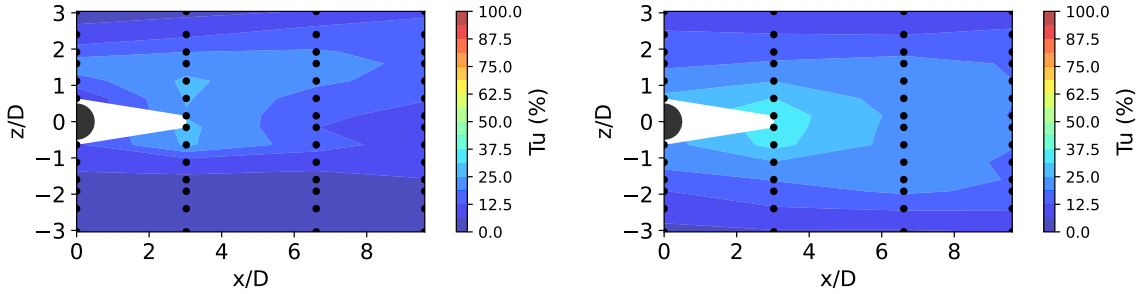

(a) Re = 300. (b) Re = 1800.

Figure 10. Turbulence intensity downstream of two unit cells in series at y/D = 1.5 at different Reynolds numbers.

Figure 11 shows the wake of two unit cells in series at the plane $y/D = 0.5$. At $Re = 300$, the wake contains singular, more turbulent flow compared to the single unit cell and the split turbulent zones present behind the first unit cell are disrupted by the second unit cell in the series to produce one larger zone. The max turbulence intensity in the wake of two unit cells at $Re = 300$ is around 84% whereas the single unit cell maxes out at around 70%. This wake, similar to the wake at $Re = 300$ and $y/D = 1.5$, is asymmetric but in contrast, it is more turbulent. At $Re = 1800$, the wake becomes mostly symmetric after transitioning in the range $300 < Re < 1800$ and is slightly less turbulent (max 46%) when compared to the single unit cell (max 50%) under the same conditions and positions. The highly turbulent zone of around 40% intensity is also wider behind the single unit cell but the approaching flow, again is more turbulent approaching the second unit cell.

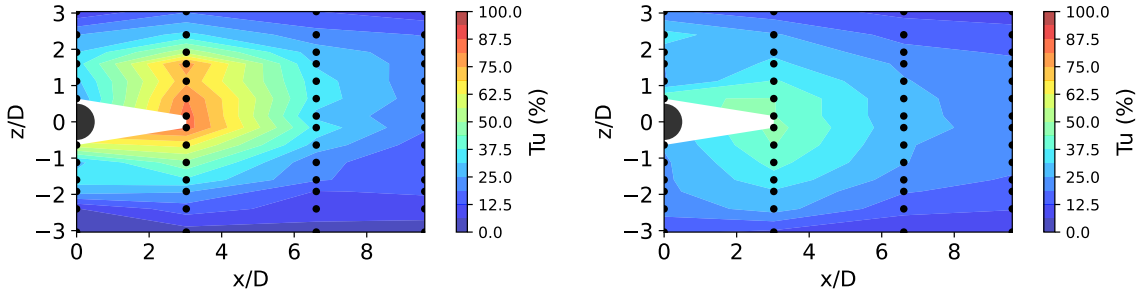

(a) Re = 300. (b) Re = 1800.

Figure 11. Turbulence intensity downstream of two unit cells in series at y/D = 0.5 at different Reynolds numbers.

The two unit cells in series have only the downstream unit cell coated with only four naphthalene coated trusses. The Sherwood numbers for each truss based on the diameter of the truss at the various Reynolds numbers are shown in Figure 12a. Trusses 1, 3 and 4 all have similar Sherwood numbers at each Reynolds number and similarly to the single unit cell, truss 2 has lower Sherwood numbers if basing it on the diameter of the truss. Although the flow at $Re = 300$ is asymmetric, there only seems to be a small increase in Sherwood number at truss 1 compared to trusses 3 and 4; however, this increase is also within the uncertainty of the Sherwood number. If using the diameter as the characteristic length for the Sherwood number calculation, trusses 1, 3, and 4 perform 24–40%. 17–42%, and 20–24% better than a cylinder in cross flow, respectively. Truss 2 performs 5-18% better than a cylinder in crossflow beginning at $Re = 1200$. A better transfer when compared to a cylinder is most likely due to the approaching velocity field incorporating more turbulence and larger mixing zones in the downstream flow behind the second unit cell. If using the characteristic length as the length downstream when calculating the Sherwood number for truss 2, it performs significantly (108–169%) better than a turbulent flat which is shown in Figure 12b. At $y/D = 0.5$, which is right above truss 2, there is a significant turbulence increase and adding that to an already turbulent approaching flow will cause a better transfer over that truss when compared to a flat plate.

3.3. THREE UNIT CELLS IN SERIES

The wake behind three unit cells in series is quite similar to the flow behind two unit cells. At $y/D = 1.5$ (Figure 13), the wake behind the three unit cells in series, although more turbulent (maximum around 44%), displays a similar asymmetry with the more turbulent region on the positive z/D axis. The approaching flow displays some turbulence as well. The wake behind three unit cells at $Re = 1800$ is much more similar to the wake of the two unit cells in series at the same conditions in the area closer to the unit cell. Both have around

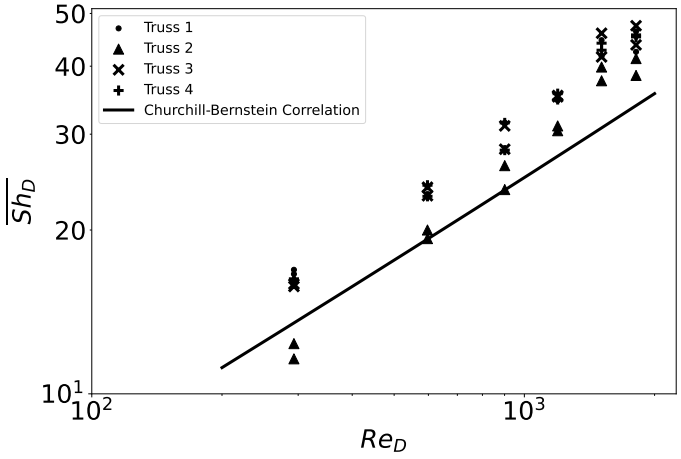

(a) Sherwood number based on the diameter of the trusses.

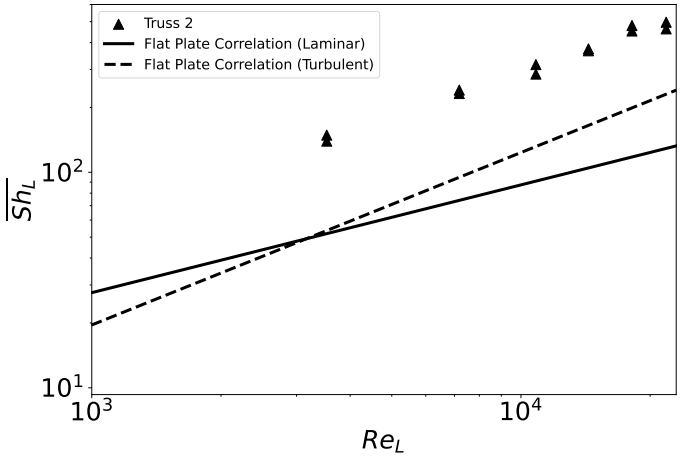

(b) Sherwood number based on the distance downstream relative to truss 5 upstream on the single unit cell.

Figure 12. Sherwood number for the various trusses of the two unit cells in series configuration.

the same maximum turbulence intensity at 35% and similarly sized and shaped turbulent regions. The only difference is further downstream of the three unit cells in series at around $x/D = 6.6$ there is an anomaly where there is a point of reduced turbulence. The flow also has adjusted to a relatively symmetrical flow at $Re = 1800$ despite the deviation in the -z/D axis farther downstream.

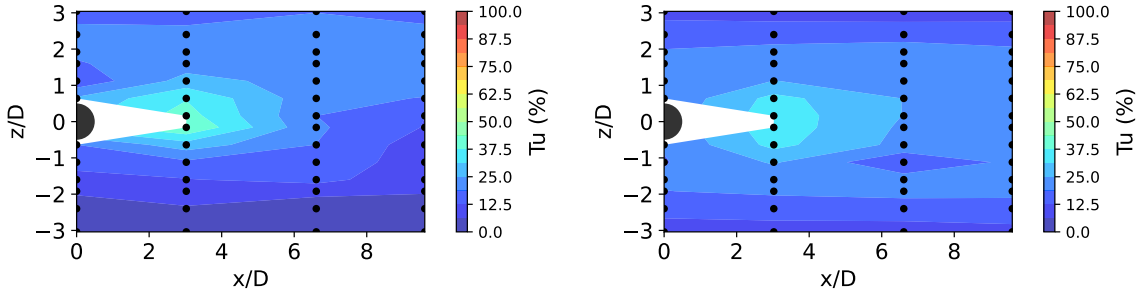

(a) Re = 300. (b) Re = 1800.

Figure 13. Turbulence intensity downstream of three unit cells in series at y/D = 1.5 at different Reynolds numbers.

The turbulent wake at $y/D = 0.5$ is shown in Figure 14. The flow at $Re = 300$ is relatively symmetrical compared to the wake behind the two unit cells. The wake is also smaller but more turbulent reaching around 125% compared to the two unit cell configuration's 84% turbulent intensity. The approaching flow is also slightly more turbulent at around 20% for the three unit cells and 15% for the two unit cells. This increase in turbulence is most likely due to the increased mixing behind an additional unit cell. At $Re = 1800$, the turbulent wake is symmetric and has a similarly sized and shaped wake compared to the two unit cells under the same conditions. Along the $x/D = 0$ line, there is the same increase in turbulence at around $z/D \approx 2.5$ but then also has an increase at around $z/D \approx -2.5$ as well which isn't present in the two unit cells' wake. Similar to the two unit cell configuration and unlike the single unit cell, the turbulence intensity is higher near where the trusses meet at the center point ($y/D = 0.5$) compared to halfway up truss 4 ($y/D = 1.5$)

Similar to the two unit cells in series, the three unit cells in series has four coated trusses on the back unit cell. The Sherwood number results based on the diameter are shown in Figure 15a. Trusses 1, 3, and 4 have better mass transfer than truss 2 and a singular cylinder in crossflow at all Reynolds number, and similarly to the two unit cells in series, the approaching flow contains some turbulence and has a larger, more intense

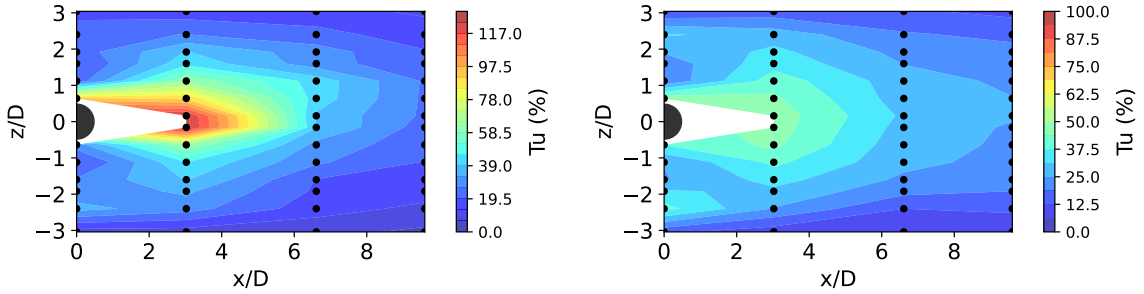

(a) Re = 300. (b) Re = 1800.

Figure 14. Turbulence intensity downstream of three unit cells in series at y/D = 0.5 at different Reynolds numbers.

mixing zone behind the unit cell compared to a single cylinder in crossflow. This results in a 20–32%, 25–32%, and 25–31% increase in Sherwood number compared to a cylinder. Truss 2 has lower mass transfer at $Re = 300$ when compared to the cylinder correlation, but unlike the two unit cells in series which starts to consistently perform better than a cylinder at $Re = 1200$, the three unit cell configuration's truss 2 has a consistently better transfer over a cylinder beginning at $Re = 600$. This truss 2 has a 4–20% increased transfer over a cylinder. This better transfer at a lower Reynolds is likely due to higher turbulent mixing zones behind the three unit cells in series right above truss 2 at $y/D = 0.5$. This exceeds 100% at $Re = 300$. If comparing truss 2 to a flat plate, it performs significantly than the laminar flat plate correlation and 130–196% better than the turbulent flat plate correlation which can be seen in Figure 15b and is due to the high turbulence zone near right above the truss seen in Figure 14.

If comparing all three unit cell configurations' transfer Figure 16 over the area of the naphthalene coated trusses 1, 2, 3, and 4 and basing the Sherwood number on the diameter of the truss, there is only a little performance reduction when changing from one unit cell to two and three in series. The single unit cell, although within the uncertainty, has a better transfer than the other two configurations at $Re \geq 900$ but performs similarly at $Re = 300$ and $Re = 600$ and this is due to lower transfer rate for truss 2 on the single unit cell when

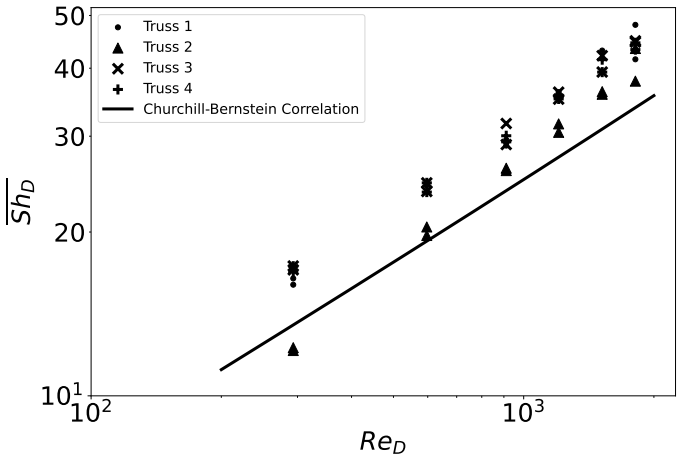

(a) Sherwood number based on the diameter of the trusses.

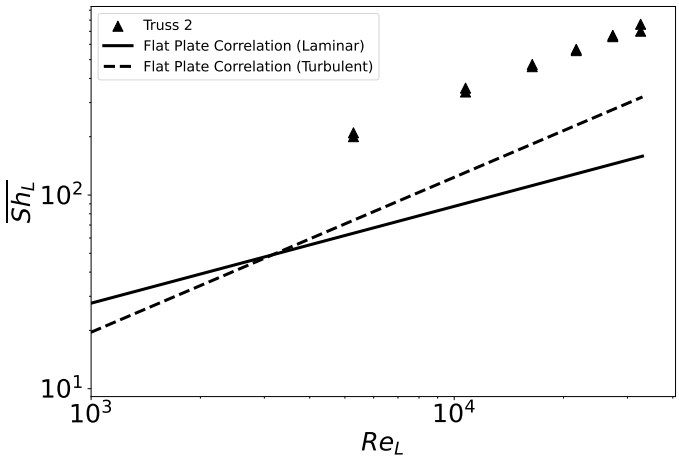

(b) Sherwood number based on the distance downstream relative to truss 5 upstream on the single unit cell.

Figure 15. Sherwood number for the various trusses of the three unit cells in series configuration.

compared to truss 2 on the two and three in series at the lower Reynolds numbers. There is an expected loss in efficiency due to the reduction in velocity even though the approaching flow is more turbulent for the two and three in series. This can be seen in the percent increase in Sherwood number when comparing each configuration to a cylinder. Overall, the single unit has about a 16–42% increase whereas the two and three in series have a

12–29% and 16–29% increase, respectively. Both the two unit cells and three unit cells in series downstream unit cell perform similarly without any noticeable difference between the two at all Reynolds numbers within the uncertainty.

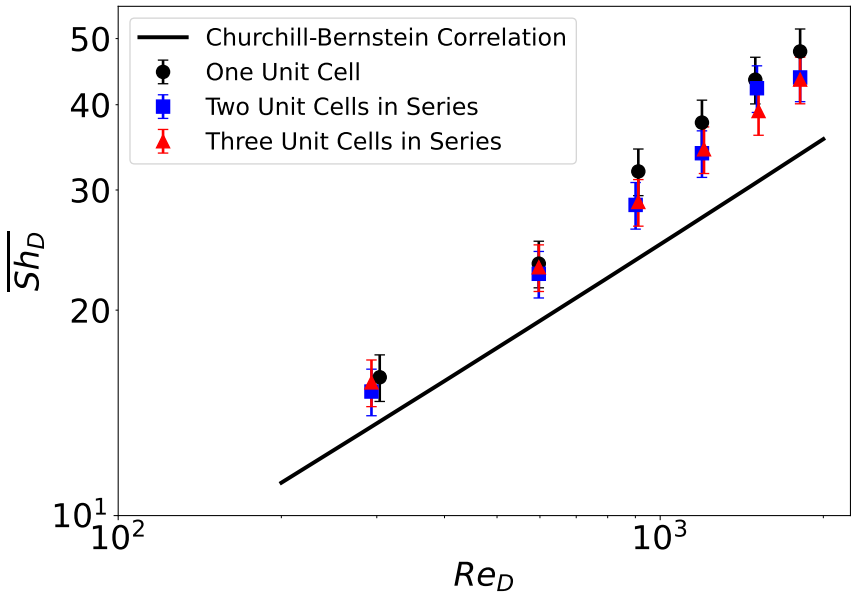

Figure 16. All three unit cell configurations averaged over the entire naphthalene coated parts compared to the Churchill-Bernstein Correlation.

4. CONCLUSIONS

In this work, the area average surface transport coefficients were studied in several unit cell geometry configurations such as a single unit cell, two in series, and three in series. A somewhat localized transport coefficient could be investigated in each truss due to the utilization of additive manufacturing and the naphthalene sublimation technique. To aid in the investigation of the transport coefficient, the unit cell wake is also studied at various points downstream of the unit cell configurations.

The single unit cell's trusses 1, 3, and 4 which are better compared to a cylinder in crossflow due to their orientation on the unit cell, have better performance in the Reynolds number range 300–1800 and although in a different orientation, truss 2 gets consistently better mass transfer which correlates to better heat transfer than a cylinder at $Re \geq 900$.

The two and three unit cells in series perform similar in terms of mass transfer. In both configurations, trusses 1, 3, and 4 get better transfer over the entire Reynolds number range, but truss 2 on the two unit cells in series consistently gets better transfer compared to a cylinder at $Re \geq 1200$ compared to the three in series' better transfer at $Re \geq 900$. Truss 2 (and the singular truss 5), if comparing to a flat plate due to its orientation on the unit cell, and treating each truss 2 on each unit cell configuration as a continuation of the flat plate by using its additive length as the characteristic length, gets better transfer in the Reynolds number range from ~1500 to ~32600.

ACKNOWLEDGEMENTS

This project was supported by the Department of Energy's Kansas City National Security Campus.

REFERENCES

[1] H. J. Xu, Z. G. Qu, T. J. Lu, Y. L. He, and W. Q. Tao. Thermal modeling of forced convection in a parallel-plate channel partially filled with metallic foams. *Journal of Heat Transfer*, 133(9), jul 2011. doi: 10.1115/1.4004209.

[2] Henk Huisseune, Sven De Schampheleire, Bernd Ameel, and Michel De Paepe. Comparison of metal foam heat exchangers to a finned heat exchanger for low reynolds number applications. *International Journal of Heat and Mass Transfer*, 89:1–9, oct 2015. doi: 10.1016/j.ijheatmasstransfer.2015.05.013.

[3] Chih-Cheng Chen, Po-Chuan Huang, and Hsiu-Ying Hwang. Enhanced forced convective cooling of heat sources by metal-foam porous layers. *International Journal of Heat and Mass Transfer*, 58(1-2):356–373, mar 2013. doi: 10.1016/j.ijheatmasstransfer.2012.11.041.

[4] Mo Bai and J.N. Chung. Analytical and numerical prediction of heat transfer and pressure drop in open-cell metal foams. *International Journal of Thermal Sciences*, 50(6):869–880, jun 2011. doi: 10.1016/j.ijthermalsci.2011.01.007.

[5] A. Tamayol and K. Hooman. Thermal assessment of forced convection through metal foam heat exchangers. *Journal of Heat Transfer*, 133(11), sep 2011. doi: 10.1115/1.4004530.

[6] Shadi Mahjoob and Kambiz Vafai. A synthesis of fluid and thermal transport models for metal foam heat exchangers. *International Journal of Heat and Mass Transfer*, 51 (15-16):3701–3711, jul 2008. doi: 10.1016/j.ijheatmasstransfer.2007.12.012.

[7] W. Lu, C.Y. Zhao, and S.A. Tassou. Thermal analysis on metal-foam filled heat exchangers. part i: Metal-foam filled pipes. *International Journal of Heat and Mass Transfer*, 49(15-16):2751–2761, jul 2006. doi: 10.1016/j.ijheatmasstransfer.2005.12.012.

[8] C.Y. Zhao, W. Lu, and S.A. Tassou. Thermal analysis on metal-foam filled heat exchangers. part II: Tube heat exchangers. *International Journal of Heat and Mass Transfer*, 49(15-16):2762–2770, jul 2006. doi: 10.1016/j.ijheatmasstransfer.2005.12.014.

[9] J.-J. Hwang, G.-J. Hwang, R.-H. Yeh, and C.-H. Chao. Measurement of interstitial convective heat transfer and frictional drag for flow across metal foams. *Journal of Heat Transfer*, 124(1):120–129, may 2001. doi: 10.1115/1.1416690.

[10] V. V. Calmidi and R. L. Mahajan. Forced convection in high porosity metal foams. *Journal of Heat Transfer*, 122(3):557–565, feb 2000. doi: 10.1115/1.1287793.

[11] John Banhart. Manufacture, characterisation and application of cellular metals and metal foams. *Progress in Materials Science*, 46(6):559–632, jan 2001. doi: 10.1016/S0079-6425(00)00002-5.

[12] Burhan Ozmat, Bryan Leyda, and Burton Benson. Thermal applications of open-cell metal foams. *Materials and Manufacturing Processes*, 19(5):839–862, oct 2004. doi: 10.1081/LMMP-200030568.

[13] Uzair Sajjad, Tauseef ur Rehman, Mubasher Ali, Cheol Woo Park, and Wei-Mon Yan. Manufacturing and potential applications of lattice structures in thermal systems: A comprehensive review of recent advances. *International Journal of Heat and Mass Transfer*, 198:123352, dec 2022. doi: 10.1016/j.ijheatmasstransfer.2022.123352.

[14] Inderjot Kaur and Prashant Singh. Critical evaluation of additively manufactured metal lattices for viability in advanced heat exchangers. *International Journal of Heat and Mass Transfer*, 168:120858, apr 2021. doi: 10.1016/j.ijheatmasstransfer.2020.120858.

[15] T. Kim, C.Y. Zhao, T.J. Lu, and H.P. Hodson. Convective heat dissipation with lattice-frame materials. *Mechanics of Materials*, 36(8):767–780, aug 2004. doi: doi:10.1016/j.mechmat.2003.07.001.

[16] T. Kim, H.P. Hodson, and T.J. Lu. Contribution of vortex structures and flow separation to local and overall pressure and heat transfer characteristics in an ultralightweight lattice material. *International Journal of Heat and Mass Transfer*, 48(19-20):4243–4264, sep 2005. doi: 10.1016/j.ijheatmasstransfer.2005.04.026.

[17] Beibei Shen, Yang Li, Hongbin Yan, Sandra K.S. Boetcher, and Gongnan Xie. Heat transfer enhancement of wedge-shaped channels by replacing pin fins with kagome lattice structures. *International Journal of Heat and Mass Transfer*, 141:88–101, oct 2019. doi: 10.1016/j.ijheatmasstransfer.2019.06.059.

[18] Liang Xu, Hanghang Chen, Lei Xi, Yanhong Xiong, Jianmin Gao, and Yunlong Li. Flow and heat transfer characteristics of a staggered array of kagome lattice structures in rectangular channels. *Heat and Mass Transfer*, 58(1):41–64, jun 2021. doi: 10.1007/s00231-021-03100-2.

[19] H.B. Yan, Q.C. Zhang, T.J. Lu, and T. Kim. A lightweight x-type metallic lattice in single-phase forced convection. *International Journal of Heat and Mass Transfer*, 83: 273–283, apr 2015. doi: 10.1016/j.ijheatmasstransfer.2014.11.061.

[20] J.Y. Ho, K.C. Leong, and T.N. Wong. Additively-manufactured metallic porous lattice heat exchangers for air-side heat transfer enhancement. *International Journal of Heat and Mass Transfer*, 150:119262, apr 2020. doi: 10.1016/j.ijheatmasstransfer.2019.119262.

[21] Aniket Chaudhari, Pawankumar Ekade, and Shankar Krishnan. Experimental investigation of heat transfer and fluid flow in octet-truss lattice geometry. *International Journal of Thermal Sciences*, 143:64–75, sep 2019. doi: 10.1016/j.ijthermalsci.2019.05.003.

[22] Justin Broughton and Yogendra K. Joshi. Comparison of single-phase convection in additive manufactured versus traditional metal foams. *Journal of Heat Transfer*, 142 (8), jun 2020. doi: 10.1115/1.4046972.

[23] R.J. Goldstein and H.H. Cho. A review of mass transfer measurements using naphthalene sublimation. *Experimental Thermal and Fluid Science*, 10(4):416–434, may 1995. doi: https://doi.org/10.1016/0894-1777(94)00071-F.

[24] D. Ambrose, I.J. Lawrenson, and C.H.S. Sprake. The vapour pressure of naphthalene. *The Journal of Chemical Thermodynamics*, 7(12):1173–1176, dec 1975. doi: 10.1016/0021-9614(75)90038-5.

[25] Cho Keumnam, Thomas F. Irvine, and Jacob Karni. Measurement of the diffusion coefficient of naphthalene into air. *International Journal of Heat and Mass Transfer*, 35(4):957–966, apr 1992. doi: 10.1016/0017-9310(92)90260-Y.

[26] S. W. Churchill and M. Bernstein. A correlating equation for forced convection from gases and liquids to a circular cylinder in crossflow. *Journal of Heat Transfer*, 99(2): 300–306, may 1977. doi: 10.1115/1.3450685.

[27] Frank P. Incropera. *Fundamentals of heat and mass transfer.* Wiley, sixth edition, 2006. ISBN 9780471457282.

II. AREA AVERAGE SURFACE TRANSFER COEFFICIENTS IN AN ARRAY OF UNIT CELLS

Benjamin Mackey & K. O. Homan
Department of Mechanical & Aerospace Engineering
Missouri University of Science and Technology
Rolla, Missouri 65409–0050
Tel: 573–341–6622, Fax: 573–341–4115
Email: khoman@mst.edu

ABSTRACT

Lattices structures are a way to provide heat transfer enhancement and are usually made of repeated patterns of a geometry called a unit cell. In this study, a unique and simple geometry is chosen for the unit cell and four different trusses are studied in the center unit cell in a 3x3 unit cell array. The surface transport is found experimentally using a combination of additive manufactured parts and the naphthalene sublimation technique in a 300–1800 Reynolds number range in 300 Re intervals. The surface transport is analyzed regionally by examining the transport off each truss and also averaged over the entire naphthalene coated parts of the unit cell. The Sherwood numbers of all trusses are compared to the transfer from a cylinder in crossflow and two trusses, due to the orientation in the wind tunnel, are also compared to laminar and turbulent transfer from a flat plate. The wake behind the center unit cell is also studied using hot wire anemometry at several locations downstream of the center unit cell. The center unit cell gets 5–34% better transfer than a single cylinder in crossflow and performs similarly to a single unit cell. If comparing trusses 2 and 4 to a turbulent flat plate, then they are getting 178–228% and 37–63% increase in Sherwood number, respectively. These unit cell geometries can improve mass transfer and therefore heat transfer in a lower Reynolds number range and get increasingly better transfer as the Reynolds number increases.

Keywords: forced convection, naphthalene sublimation, unit cell array, lattices, mass transfer, hotwire anemometry

1. INTRODUCTION

There is constant necessity for improvements to heat transfer enhancement in various engineering applications. Some of these improvements include better efficiency, the ability to be customized for specific needs, and enhanced heat transfer. Current and improving technologies include cellular materials which cover a variety of different types such as porous and lattice structures. These provide heat transfer enhancement through their relatively high surface area and ability to produce higher turbulence and better fluid mixing. A popular porous structure is an open-cell metal foam usually constructed with highly conductive metal such as aluminum or copper and made up of randomly distributed pores supported by various sized struts. Metal foams are desirable due to their low density, large surface area, an ability to provide better fluid mixing, high thermal conductivity, and high strength [1]. Many studies have been done that demonstrate increased heat transfer performance, but at the cost of a higher pressure drop [1–10]. Open cell metal foams can be used for many different applications including heat exchangers and heat sinks, but they can also be used in applications that can incorporate the mechanical properties into designs including transportation, aerospace, biomedical, and construction [11, 12].

Due to recent advances in additive manufacturing, various types of lattice structures have been developed and studied for various applications. Sajjad et al. [13] and Kaur and Singh [14] provide comprehensive reviews on studies with various unit cell geometries and the different additive manufacturing techniques used in the creation of the lattice structures. A lattice is a structure made up of a repeated pattern of geometries called unit cells and these unit cells are usually designed with cylindrical struts or trusses. Some unit cell

topologies include tetrahedral, Kagome, pyramidal, and X-type and unlike metal foams, these topologies can be customized with different ratios and dimensions, and new unique geometries can be developed by utilizing different additive manufacturing techniques.

An early study by Kim et al. [15] looked at convective heat transfer from lattice frame materials (LFM) by developing a sandwich style heat sink comprised of these LFMs. The LFMs performed similarly to a bank of staggered cylinders and removed six times more heat than an empty channel due to the porosity which promotes turbulent flow. Kim et al. [16] did another study on the flow structures created by these LFMs using a tetrahedral unit cell. The dominant flow features include horseshoe-shaped vortices that form in front of the vertices of LFM and arch-shaped vortices that form behind the vertices. The horseshoe vortex increased heat transfer by up to 180% more than locations where the horseshoe vortex wasn't present in the end wall region. The arch vortex creates regions of recirculating and reattachment which also contributes to a higher heat transfer, and the regions before the flow separation produced around 40% of the total heat transfer in the LFM. The LFMs, although overall they produce lower heat transfer than most metal foams and packed beds, the thermal efficiency is better than the foams and other heat transfer media.

Of the various unit cell topologies, Shen et al. [17] researched the Kagome topology and the effect of replacing pin fin arrays with it in wedge shaped channels. The model with the three arrays of Kagome lattices produced 9 – 28%, 6–25%, and 16–71% higher Nusselt numbers than the models with the two arrays of pin fins, two arrays of Kagome lattices and three arrays of pin fins, respectively. The two arrays of Kagome lattices and two arrays of pin fins performed similarly, and the three arrays of pin fins performed the worst in terms of heat transfer performance. Despite the differences in thermal performance, the pressure loss was the same at the same Reynolds number and porosity in all models. Xu et al. [18] took the same Kagome topology and looked at changing different parameters of the geometry to possibly optimize it. Both increasing the inlet Reynolds number and increasing the diameter of the truss column can improve the heat transfer performance. Increasing the

ratio of column diameter to channel height from 0.1 to 0.6 results in the Nusselt number of the channel wall increasing by 32.2%. Increasing both the inclination angle and included angle in the Kagome lattice resulted in a lower Nusselt number. Shen et al. [19] looked at the performance of two different types of Kagome: cast and wire woven bulk (WBK) sandwich panels. The cast sandwich panel's overall Nusselt was 26-31% higher than the WBK even though the pressure drop is similar.

Another type of topology is the x-type unit cell. Yan et al. [20] studied the performance of x-type compared to LFM and Kagome geometries. When using the same material and porosity for each geometry, the x-type produced up to 170% and 100% better heat transfer enhancement than an LFM and Kagome, respectively, and when comparing thermal efficiency at a fixed pumping power, the x-type performs better compared to the LFM and Kagome geometries. Yan et al. [21] then looked at using the x-type topology in a ventilated brake disc. When testing within the operating range of a passenger vehicle, the brake disc with the x-type lattices performed 18–21% and better than a radial vane brake disc in terms of steady state overall Nusselt number even though it reduced pumping capacity by 40%. Xi et al. [22] studied different ways of changing the parameters of the x-type unit cell and their effects on heat transfer performance in a cooling channel. The different parameters include inlet Reynolds number, ratio of truss diameter to channel height, ratio of transverse spacing to characteristic length of the truss and the ratio of streamwise spacing to characteristic length of the truss. Increasing the inlet Reynolds number increased the heat transfer coefficient, increasing the ratio of truss diameter to channel height from 0.1 to 0.3, increased the Nusselt number by 57.5–87.9%, increasing the ratio of transverse spacing to characteristic length from 1 to 3, decreased the Nusselt number by 44.9–57.7% and increasing the ratio of streamwise spacing to characteristic length, first increased and then decreased Nusselt number.

There have been many advances in additive manufacturing (AM) which can allow for more complex geometries to be experimentally tested and previous topologies to be modified. Ho et al. [23] used selective laser melting to create heat exchangers with different sized unit cells. With the aid of AM, they were able to create two lattices, 7 mm and 14 mm. The smaller lattice produced 40–45% higher overall thermal conductance values when compared to the larger one. When comparing to fin-tube heat exchangers, the lattice heat exchangers had two times higher air side heat transfer coefficient at the same mass flow rate of air. Liang et al. [24] also used selective laser melting to experimentally test four different types of unit cells: body centered cubic (BCC), face centered cubic (FCC), x-type, and Kagome. In this experiment and in terms of thermal efficiency, the BCC lattice was the best. The x-type, Kagome, and pin fin array performed similarly with a small reduction in thermal efficiency compared to the BCC and the FCC lattice cell performed the worst. Broughton and Joshi [25] used direct metal laser sintering to create a lattice made up of rhombic dodecahedron unit cells to compare to traditional metal foams. The Nusselt number for the rhombic dodecahedron lattice was around 60% higher compared to the metal foam; however, this came at a 60% higher pressure drop. Despite the higher pressure drop, the lattice had better thermal performance as a function of pumping power.

Lattices can provide improved heat transfer enhancement and due to advances in additive manufacturing, they can be highly customized. The paper presents a novel and simple unit cell geometry to be used in a 3x3 array. This experimental approach provides a way to find a somewhat localized mass transfer coefficients in the central unit cell in the 3x3 array at. The combination of the naphthalene sublimation technique and AM allows for the ability to capture the mass transfer from individual trusses in the unit cell. The first objective of this paper is to obtain the Sherwood number off four trusses in the middle unit cell in a lower Reynolds number range. The second objective is to experimentally obtain the turbulence intensity data from a hot wire anemometer. The hot wire data will aid in the

analysis of the mass transfer results. Together, this will provide key analysis for the chosen unit cell geometry and can support future studies for changing different parameters of the unique geometry.

2. METHODS AND APPARATUS

2.1. NAPHTHALENE SUBLIMATION TECHNIQUE

A unit cell, as referred to in this paper is made of three cylinders in each axial direction. In this experiment, a 3x3 array is comprised of unit cells with cylinders having an L/D = 6. To get a 3x3 array and due to the area restrictions by the wind tunnel, the diameter of the cylinders is around 0.425 inches which makes the length 2.55 inches. The array of unit cells is designed with an outer frame and is broken up into three main parts with four detachable trusses. The exploded view is shown in Figure 2a with numbered trusses. Each part and truss is attached via metal dowel pins. The combined unit cell array is shown in Figure 2b. The detachable trusses include a 0.084 inch recess to mold naphthalene to the surface. The frame has a clover like attachment that is inset into the test section of the wind tunnel to prevent rotation during testing. The diagram of the wind tunnel is shown in Figure 1. The parts of the array and unit cell trusses are printed using an AM technique called selective laser sintering (SLS) with nylon 12.

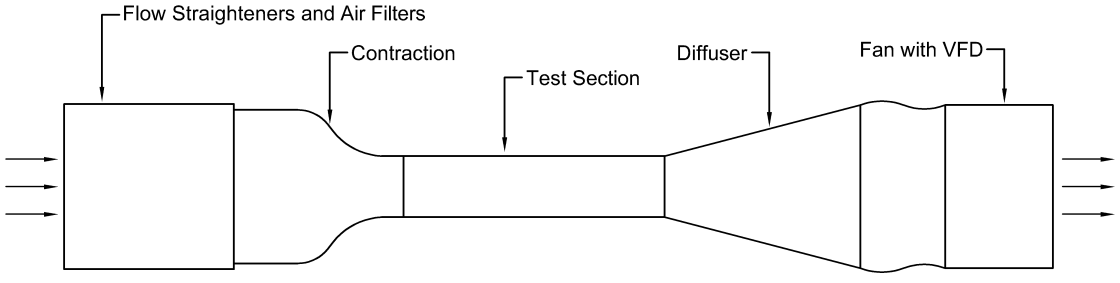

Figure 1. Wind tunnel setup.

Once the design of the unit cell is completed, a mold is needed to attach the naphthalene to the detachable unit cell trusses. The aluminum mold, shown in Figure 3b, has a runner and filling hole for each truss and can mold eight trusses in a single molding process. The ability to mold eight at one time allows for buffer in case of a molding error and if the molding process is flawless, then there are enough molded naphthalene trusses for two runs in the wind tunnel. The mold is machined with a smooth inner surface to produce an overall smooth naphthalene surface.

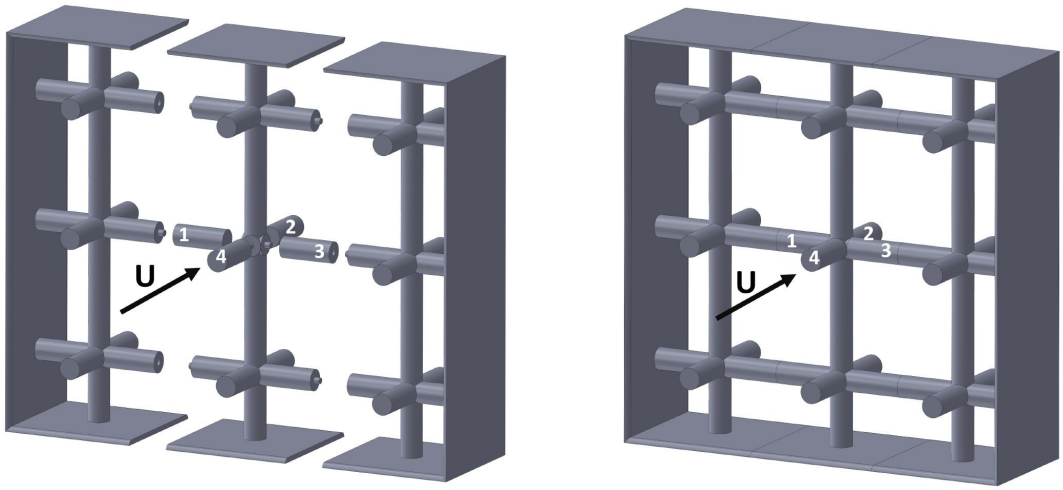

(a) Exploded view of the 3x3 array of unit cells with numbered trusses.

(b) Combined array of unit cells with numbered trusses.

Figure 2. 3x3 unit cell array diagrams.

The first part of the molding process involves melting down moth balls with a purity of 99.95% naphthalene using an IKA C-MAG HS 7 hot plate. The hot plate is set to 450 degrees C. Once the naphthalene reaches its boiling point, it is taken off the hot plate and allowed to settle for 30 seconds to stop the boiling. The molten naphthalene is poured into the mold and allowed to sit for about an hour to allow the molten naphthalene to reach room temperature. To get the trusses out of the mold, one half of the mold is hit with a hammer to create a shearing force on the naphthalene surface (recommended by Goldstein and Cho

[26]). The runners are carefully cut off to achieve a cylindrical surface profile. The trusses are inspected for surface defects and if they pass the inspection, the trusses are immediately placed in a plastic bag with a few moth balls to slow the sublimation process and preserve the cylindrical naphthalene surface. To minimize naphthalene surface temperature change, the naphthalene trusses in the bag are allowed to reach room temperature again before testing to ensure a constant temperature of the naphthalene surface throughout the whole test. Both the surface temperature and the mass of the trusses are measured separately before attaching them and putting the unit cell array in the wind tunnel. The temperature was taken using a type k thermocouple wired to an OMEGA HH82 digital thermometer which can read the temperature to an accuracy of 0.1 degrees C. The mass of each naphthalene truss is measured using a Sartorius BP211D with an accuracy of 0.01 mg. They are attached to the middle section of the array and then the middle section is sandwiched between the two other sections to complete the array. The array is set in the wind tunnel running at the desired velocity. Once the array has been inside the wind tunnel for the desired time, it is taken out of the wind tunnel, the two outside pieces are carefully pulled apart from the middle section, the naphthalene coated trusses are disconnected from the parts, and then the trusses' surface temperature and mass are taken again. The experimental test matrix for the array of unit cells is shown in Table 1.

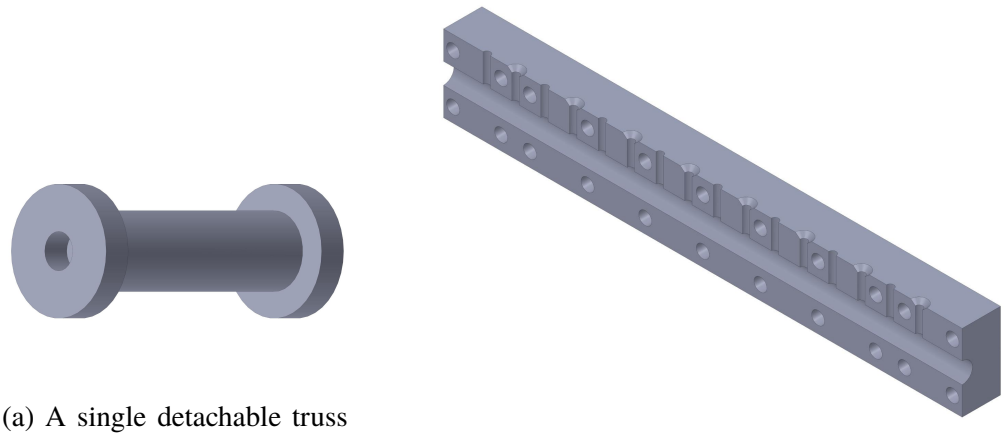

(a) A single detachable truss with naphthalene recess.

(b) Cross section of mold.

Figure 3. Molding parts.

Table 1. Unit cell array tests (U_∞ in m/s, Δm in mg, τ in minutes, T in $^\circ C$).

Re_{nom}	U_∞	Δm	τ	T
300	0.42	36.02	60.0	20.8
	0.42	27.65	45.3	20.8
600	0.85	55.72	60.3	20.9
	0.85	42.04	45.0	20.8
900	1.27	61.27	50.1	20.4
	1.27	51.05	40.0	20.2
1200	1.69	55.67	40.1	19.9
	1.69	43.85	30.2	20.0
1500	2.11	64.75	40.1	20.2
	2.11	43.56	30.1	19.5
1800	2.53	142.36	48.5	24.8
	2.53	93.41	31.4	24.7

2.2. AREA AVERAGE MASS TRANSFER COEFFICIENT CALCULATION

The area average transfer coefficient involves taking the change in the mass of the naphthalene cylinder over time and is represented by

$$\dot{m} = \frac{m_b - m_a}{\tau} \tag{1}$$

where m_b is mass of the naphthalene cylinder before the sublimation in the wind tunnel and m_a is the mass after sublimation. The mass transfer coefficient is given by

$$h_m = \frac{\dot{m}}{A_s(\rho_{v,w} - \rho_{v,\infty})} \tag{2}$$

where A_s is the surface area of the naphthalene given by $A_s = \pi DL$, $\rho_{v,w}$ is the vapor density of the naphthalene at the surface and $\rho_{v,\infty}$ is the vapor density of naphthalene in the freestream. It is assumed the density of the naphthalene in the freestream is negligible ($\rho_{v,\infty} = 0$) since the lab has significant ventilation to clear the air of any naphthalene vapor. The vapor density of the naphthalene at the surface is calculated using the ideal gas law given by

$$\rho_v = \frac{P_v}{R_{nap}T} \tag{3}$$

where R_{nap} is the individual gas constant for naphthalene ($R_{nap} = 64.871 J/kgK$) and is found by dividing the universal gas constant ($R_u = 8.3145 kJ/kmolK$) by the molar mass of naphthalene (28.17 kg/kmol). The temperature of the naphthalene surface is denoted by T and P_v is the naphthalene vapor pressure. The naphthalene vapor pressure is calculated using the correlation found by Ambrose et al. [27],

$$TlogP_v = \frac{1}{2}a_0 + \sum a_n E_n(x) \tag{4}$$

$$x = \frac{2T - 574}{114} \tag{5}$$

where $a_0 = 301.6247$, $a_1 = 791.4937$, $a_2 = -8.2536$, $a_3 = 0.4043$, $E_1(x) = x$, $E_2(x) = 2x^2 - 1$, and $E_3(x) = 4x^3 - 3x$. Then the Sherwood number, based on the characteristic length of the of the naphthalene trusses (in this experiment, depending on the orientation of the truss, $L_c = L$ or $L_c = D$), can be calculated,

$$Sh = \frac{h_m L_c}{D_f} \tag{6}$$

The diffusion coefficient of naphthalene in air, D_f, is calculated using the correlation given by Goldstein and Cho [26],

$$D_f = 0.0681 \left(\frac{T}{298.1}\right)^{1.93} \frac{1.013 \times 10^5}{P} \tag{7}$$

Once the Sherwood number is found, then the Nusselt number can be calculated from the heat and mass transfer analogy,

$$Nu = Sh \left(\frac{Pr}{Sc}\right)^n \tag{8}$$

where n can range from 1/3 to 0.4 [26] and is found from empirical results. To implement the analogy, the Schmidt number and Prandtl numbers need to be equal. In this experiment, the Schmidt number is 2.23 for naphthalene in air and the Prandtl number is 0.71 for air, but according to Goldstein and Cho [26] it can still be and has been applied with assurance. The Schmidt number can also be found more accurately by the Keumnam et al. [28] correlation,

$$Sc = 8.0743T^{-0.2165} \tag{9}$$

2.3. HOT WIRE ANEMOMETRY

To measure the average flow velocity and perform measurements of the flow behind the unit cell array, a Dantec Dynamics single wire anemometer is used. The hot wire is attached to a Dantec Systems Multichannel CTA 54N82. StreamWare Basic software is used to calibrate the hot wire and record velocity and time data. Solid unit cell configurations (without detachable trusses and naphthalene recesses) are printed to avoid possible unwanted interactions. The hot wire measurements are taken at four locations downstream of the array at $x/D = 0$, $x/D = 4.4$, $x/D = 9.7$, and $x/D = 14.1$ which is shown in Figure 4a. The x-locations are limited due to the wind tunnel setup. Fourteen hot wire data points are taken along each of those x-locations except two at $x/D = 0$ due to a truss blocking the ability to take data points in that location. That plane of points is used to take data at two different y-locations, $y/D = 0.5$ and $y/D = 1.5$ which is shown in Figure 4b. A set of data points is taken downstream of cylinder to compare to the trusses at both y-planes. Due to the difference in diameter, the non-dimensional locations behind the cylinder are slightly different at $x/D = 0, 3.0, 6.6, 9.6$. These data points are used to make a contour plot of the average velocity and turbulence intensity and due to the nature of the formation of the contour plots, there is some interpolation happening between the points.

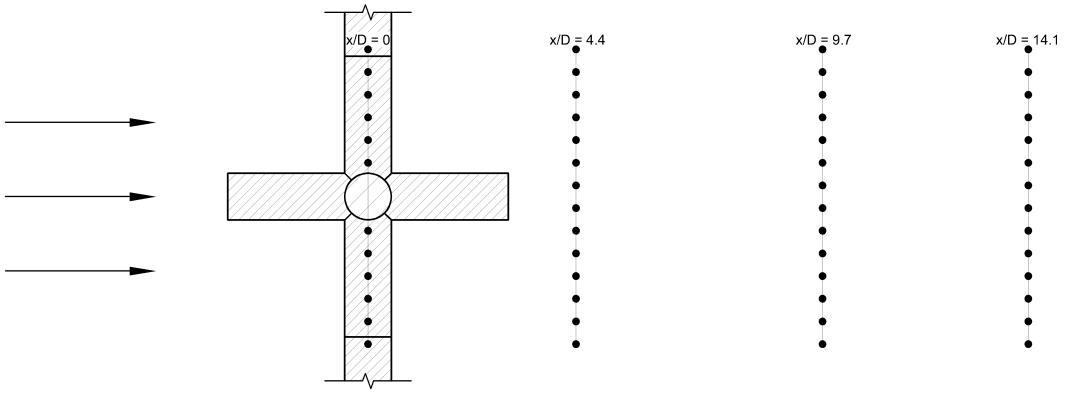

(a) Top view.

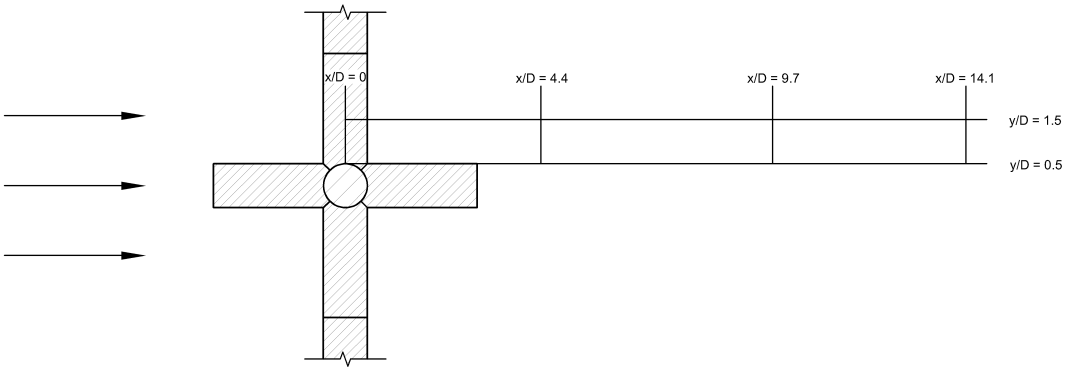

(b) Side view.

Figure 4. The different planes and data points taken using the hot wire anemometer behind the middle unit cell.

2.4. VALIDATION OF THE NAPHTHALENE SUBLIMATION TECHNIQUE

To verify the validity of the naphthalene sublimation technique as we have implemented, several circular cylinders are tested using the technique since cylinders in crossflow are well researched. The cylinders are printed using the same SLS method with a 5/8 inch diameter and similarly sized recess to mold the naphthalene to the surface. These are attached to a printed frame via a square insert to prevent rotation during testing. The cylinders are tested over a Reynolds number range of approximately 300 to 7500 which is shown in Table 2. The Sherwood numbers for the tests are shown in Figure 5 with an uncertainty of around 10.2%. The experimental results are compared to the [29] equation for cylinders in crossflow which is given by

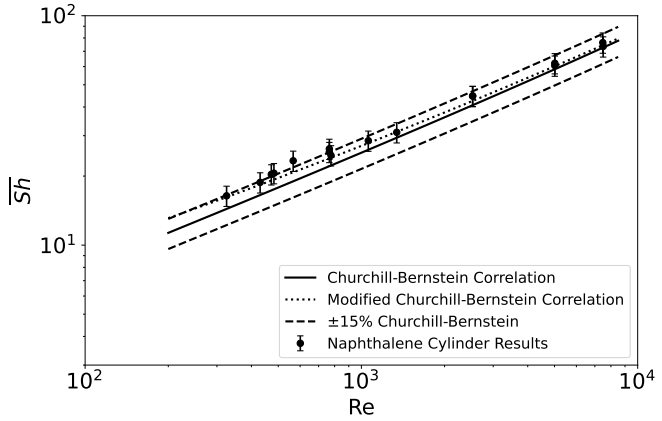

Figure 5. Comparison of naphthalene sublimation Sherwood number results to the [29] correlation.

$$\overline{Nu} = 0.3 + \frac{0.62Re^{1/2}Pr^{1/3}}{\left[1 + (0.4/Pr)^{2/3}\right]^{1/4}} \left[1 + \left(\frac{Re}{282000}\right)^{5/8}\right]^{4/5} \tag{10}$$

Using the heat and mass transfer analogy, the Churchill-Bernstein correlation can be used to find the area average Sherwood number by replacing the Prandtl with the Schmidt number so the equation becomes

$$\overline{Sh} = 0.3 + \frac{0.62Re^{1/2}Sc^{1/3}}{\left[1 + (0.4/Sc)^{2/3}\right]^{1/4}} \left[1 + \left(\frac{Re}{282000}\right)^{5/8}\right]^{4/5} \tag{11}$$

There is greater error towards the lower Reynolds number range and the paper mentions the Nu_0 (0.3 at the beginning of the equation) value or in this case the Sh_0 value is arbitrary and can be modified for any given data set. The chosen value for Sh_0 for this experimental data is 2.1 which gives a better fit; however, without changing the Sh_0, the experimental data follows the correlation quite well. The larger error in the lower Reynolds number range could also be attributed to the wide range of experimental conditions under which this equation was derived.

3. RESULTS AND DISCUSSION

To understand the experimental Sherwood number values, the flow past the unit cell and the flow past a cylinder are compared. The hot wire data is taken and converted to turbulence intensity contours. The flow past a cylinder at $Re = 300$ and $Re = 1800$ is shown in Figure 6a and Figure 6b, respectively. The cylinder produces a symmetrical wake at both Reynolds numbers and due to the smaller average streamwise velocities and larger fluctuations, the wake behind the cylinder at $Re = 300$ is significantly more unsteady.

3.1. TURBULENCE INTENSITY

The experimental data for the turbulence intensity behind the cylinder at $Re = 300$ and $Re = 1800$ is shown in Figure 6. At both Reynolds numbers, the wake is symmetrical and somewhat turbulent. At $Re = 300$, the wake reaches a max turbulence of around 64%

Table 2. Circular cylinder tests (Δm in mg, τ in minutes, T in $^{\circ}C$).

Re	Δm	Δt	T
330	110.41	90.2	21.0
430	44.92	32.1	21.0
470	175.02	121.4	20.9
480	175.35	120.2	20.8
570	177.27	120.4	20.4
760	342.27	180.0	21.4
760	160.55	85.4	21.4
780	310.65	187.6	20.8
1060	150.96	74.7	21.0
1340	99.18	45.1	21.0
2520	105.43	37.0	20.2
2520	108.95	38.3	20.2
5010	124.50	30.8	20.1
5010	129.12	32.4	20.2
7470	153.7	33.6	19.9
7490	172.3	33.5	21.0

which is due to the smaller velocities and relatively high fluctuations. At $Re = 1800$, the wake reaches a max turbulence of around 43% and grows slightly larger when compared to the wake at $Re = 300$.

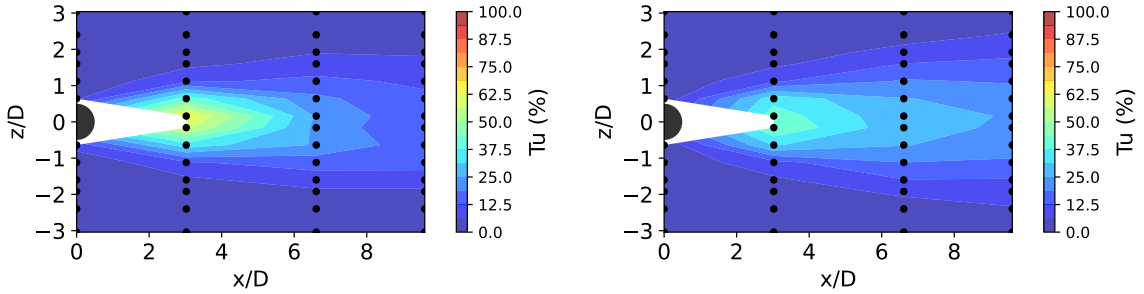

(a) Re = 300. (b) Re = 1800.

Figure 6. Turbulence intensity downstream of cylinder at different Reynolds numbers.

The wake's turbulence intensity in the y-plane $y/d = 0.5$ at $Re = 300$ and $Re = 1800$ for the center unit cell in the 3x3 unit cell array is shown in Figure 7. The wake at $Re = 300$ (Figure 7a) is symmetrical closer to the unit cell geometry and becomes somewhat less symmetrical further downstream with a slightly higher turbulence intensity near $z/D = 3$ compared to the intensity at $z/D = -3$. It most likely reaches a higher turbulence intensity closer to the array, but due to the limited available x/d locations, the max turbulence intensity at $Re = 300$ is around 50% at around $x/d = 4.4$. Compared to the single cylinder in crossflow, the max recorded turbulence intensity is lower; however, the entire wake extended from $z/D = -3$ to $z/D = 3$ includes some type of turbulence which is caused by trusses 1 and 3 since this y-plane is right above the top of those trusses. It also seems there is some interaction coming from the unit cells on the sides of the central unit cell since the turbulence intensity is high there. The turbulence intensity behind the cylinder drops off quickly whereas the the intensity going downstream of the array does not decrease as much.

At $Re = 1800$, the shape of the wake stays mostly the same with relatively high turbulence intensity near the middle and moderate turbulence intensity near the edges of the z/D axis at $x/D = 4.4$. The maximum turbulence intensity is slightly higher at around 54%

compared to 50% at $Re = 300$. Farther downstream at around $x/D = 14.1$, the turbulence intensity of the positive and negative edges of the z/D axis is slightly less, averaging around 20% whereas at $Re = 300$ it averages around 24%. Similar to the the wake at $Re = 300$ and unlike the cylinder at $Re = 1800$, the wake's turbulence at $Re = 1800$ extends out to the boundaries of the z/D axis, and the whole wake stays turbulent due to trusses 1 and 3.

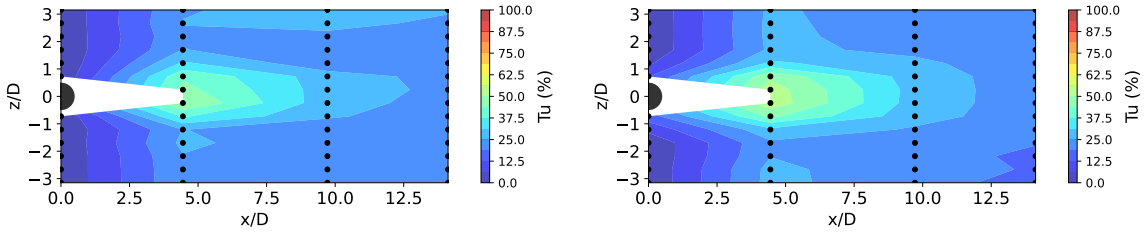

(a) Re = 300.

(b) Re = 1800.

Figure 7. Turbulence intensity downstream of 3x3 unit cell array at y/D = 0.5 at different Reynolds numbers.

The next y-plane, y/D = 1.5, is halfway up a truss and is chosen since it should exhibit similar to flow downstream of cylinder. It is tested to show any differences that might occur due to the interaction with the other possible unit cells in the array or parts of the central unit cell. The turbulence intensity at y-plane $y/D = 1.5$ is shown in Figure 8 at both chosen Reynolds numbers. At $Re = 300$ (Figure 8a), the wake is symmetrical and unlike the wake of the cylinder where it seems to reach a limit of recorded turbulence at around $z/D = -2$ and $z/D = 2$, it extends out to $z/D = -3$ and $z/D = 3$. This is likely due to interactions among the outer unit cells in the array and the various trusses in the central unit cell. The wake also only slightly drops in turbulent intensity to around 23% at $x/D \approx 10$ along the centerline ($z/D = 0$) compared to a cylinder which drops to around 13% around the same point.

When compared to the wake at $Re = 300$, the wake at $Re = 1800$ is quite similar. They both are similar in shape and symmetrical. The only difference is the maximum recorded turbulence intensity behind unit cells. At $Re = 300$, the maximum is around 30%

whereas at $Re = 1800$, the maximum is around 39%. The wake at $Re = 1800$ has the same differences to a cylinder as well. The wake extends to the boundaries of the z/D axis by the time it reaches $x/D \approx 10$ whereas the cylinder turbulence reaches to about $z/D = -2.5$ and $z/D = 2.5$ at $x/D \approx 10$. In this case, the cylinder has a higher turbulence intensity near the centerline at $x/D \approx 10$ with a value of around 24%. The wake behind the unit cell dips down to around 21%.

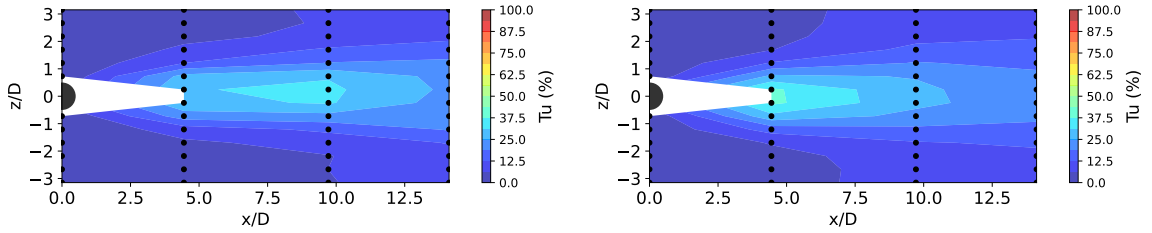

(a) Re = 300. (b) Re = 1800.

Figure 8. Turbulence intensity downstream of 3x3 unit cell array at y/D = 1.5 at different Reynolds numbers.

3.2. MASS TRANSFER

The Sherwood number of each individual truss is calculated using the diameter of the trusses and then compared to the Churchill-Bernstein equation. These results are shown in Figure 9. Trusses 1 and 3 perform similarly with a significantly higher Sherwood number than a cylinder in crossflow at every Reynolds number in the range at an increase of 38–52% and 40–51%, respectively. The higher heat transfer is most likely due to the increased turbulence intensity and mixing near where all the trusses meet since near the middle of a truss, the wake is similar to a cylinder. Truss 2, which is downstream of the intersection of the trusses, performs better than truss 4, which is upstream of the intersection, in the entire Reynolds number range. The increase in Sherwood number in truss 2 comes from the increased mixing directly above it and most likely below it due to the symmetrical nature of the wakes. Truss 4 is most likely only experience minimal mixing due to it being the first contact of the flow. Even though they are situated different than a cylinder in cross flow,

trusses 2 and 4 start performing better than a cylinder in crossflow at around $Re = 900$. Starting at $Re = 900$ and if comparing to the Churchill-Bernstein equation, truss 2 has an increase in Sherwood number of 24–44% and truss 4, starting at $Re = 1200$ (where it is consistently higher than the correlation), has an increase of 2–11%. The uncertainty of each calculated Sherwood number is around 6.1%.

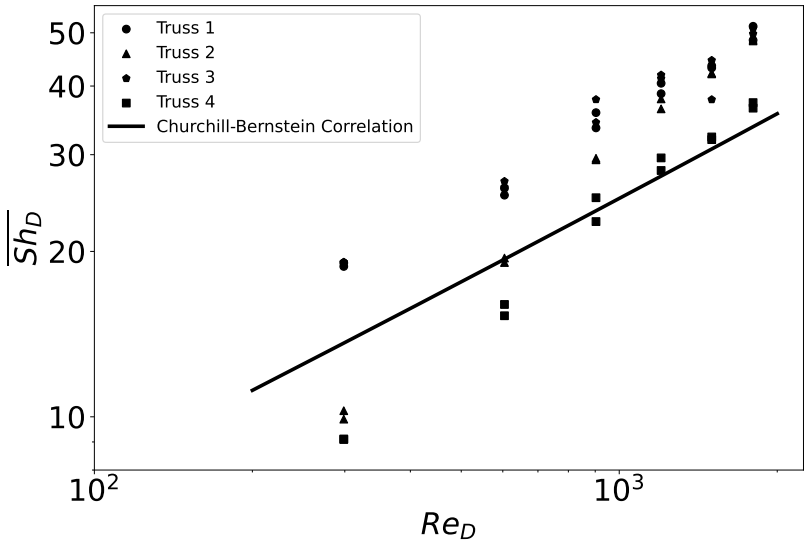

Figure 9. Sherwood number based on the diameter of the trusses in the 3x3 unit cell array configuration.

Due to the orientation of trusses 2 and 4 in the wind tunnel, two flat plate correlations [30] (laminar and turbulent) are also used to compare (Figure 10). In this experiment, truss 4 starts the flat plate and truss 2 is considered a continuation of a flat plate despite a perpendicular truss separating the two. Both trusses perform better than both flat plate conditions at every Reynolds number except for truss 4 at around $Re = 670$ where the Sherwood number is around 10% less than the correlation. Truss 2 performs significantly better than a turbulent flat plate with an increase of around 178–228%. This increased turbulence intensity seems to provide better mixing to enhance the mass transfer off truss 2.

Truss 4, despite not performing as well as truss 2, is still getting better mass transfer than even the turbulent correlation at all Reynolds numbers with an increase of 37–63%. The shape of the truss could also be contributed to the increased average Sherwood number.

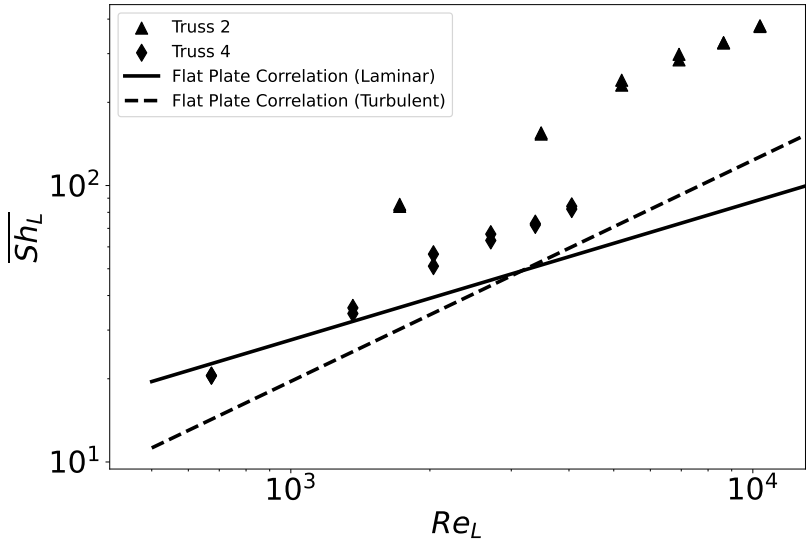

Figure 10. Sherwood number based on the distance downstream relative to truss 4 upstream.

To show the possible differences between the array and a single unit by itself, trusses 2 and 4 were compared to the single unit cell correlations obtained in another experiment (Figure 11a). In the higher Reynolds number range, 900–1800, truss 2 is getting a 6–14% increased Sherwood number possibly indicating some differences in flow caused by possible interactions in the outside unit cells in the array. In the whole Reynolds number range, truss 4 is getting a reduction (1–9%) in transfer with some outliers in one trial at $Re = 900$ and one at $Re = 1200$. Figure 11b shows the comparison of trusses 1 and 3 to their respective correlations on a singular unit cell. At $Re = 300$, both trusses on the array get better transfer than both truss correlations for the single unit cell, but all trials at higher Reynolds number perform similarly with some outliers.

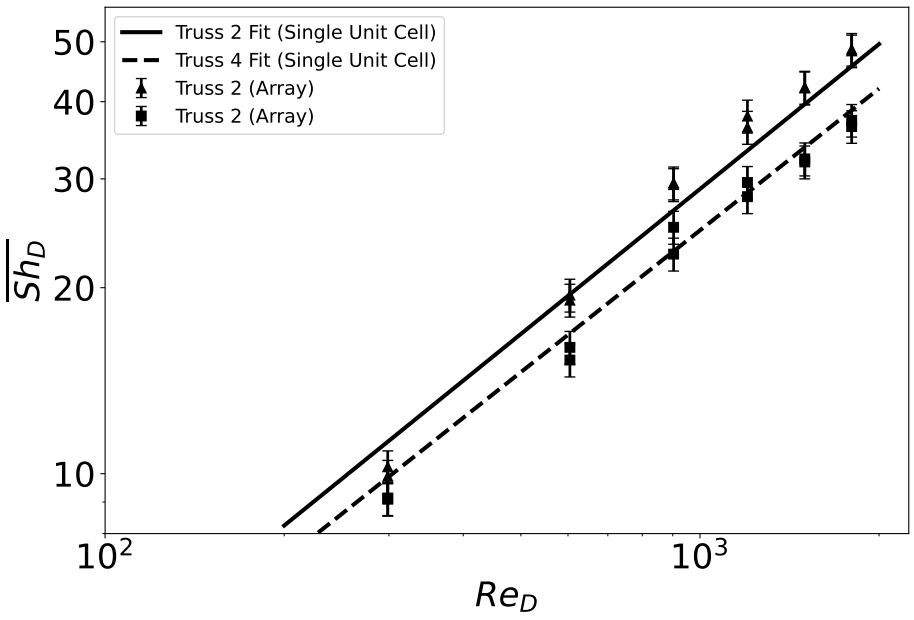

(a) Trusses 2 and 4.

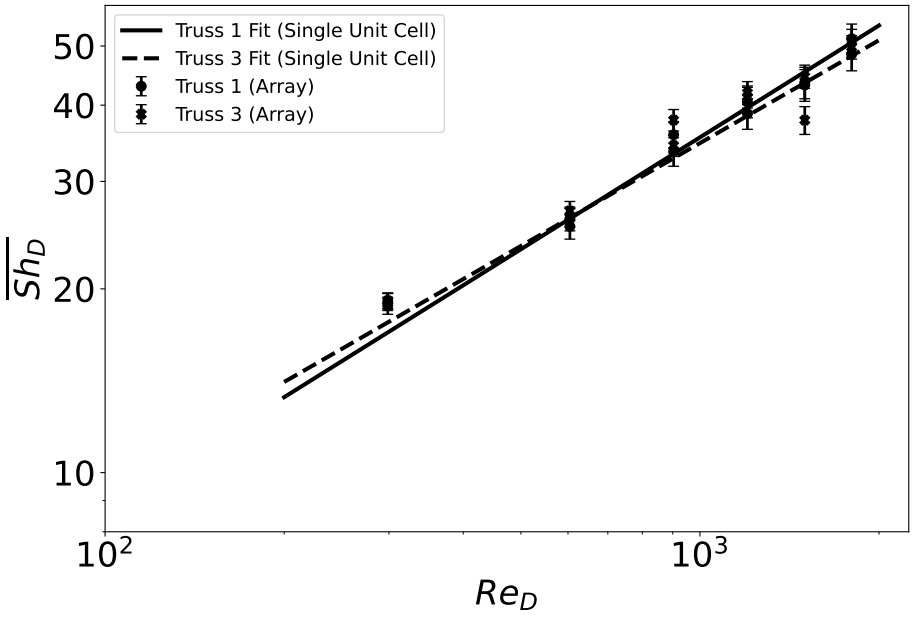

(b) Trusses 1 and 2.

Figure 11. Specific truss comparison to a single unit cell.

Figure 11b shows the overall average Sherwood number over the entire center unit cell in the array compared to the overall average on a single unit cell and the Churchill-Bernstein cylinder in cross flow correlation. Despite some differences in individual trusses, the Sherwood numbered averaged over the entire area is similar. The fit for the single unit cell could easily be a similar correlation for the overall Sherwood number for the center unit cell in the array. It seems the decrease in Sherwood number for truss 4 is dampening the increase in Sherwood number for truss 2 in the higher Reynolds number range. The somewhat localized Sherwood numbers are slightly different but the overall area average is similar to a single unit cell. If comparing the center unit cell Sherwood number to a cylinder in crossflow, then the unit cell is increasingly getting better transfer as the Reynolds number is increasing. It is getting 5–37% increase in Sherwood number over the cylinder in crossflow.

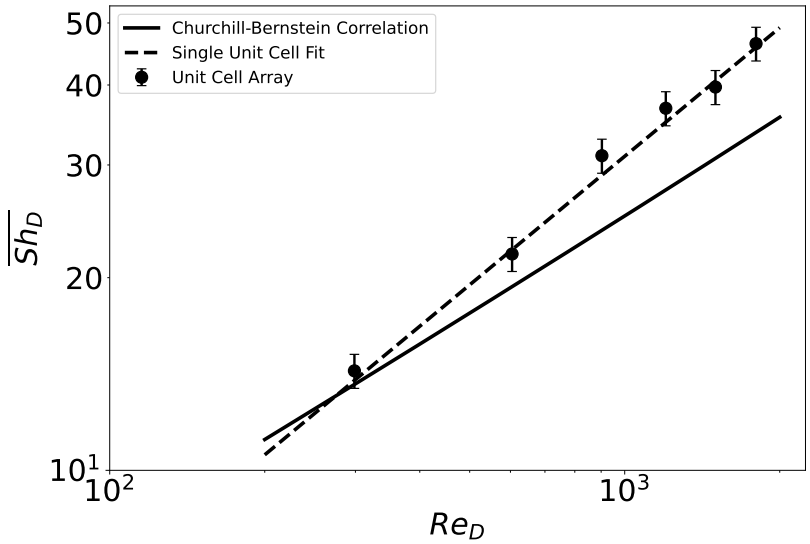

Figure 12. Sherwood number averaged over the entire naphthalene coated surface on the unit cell and between trials.

4. CONCLUSIONS

In this work, average transport coefficients were found using the naphthalene sublimation technique in the center unit cell of a 3x3 array of unit cells. A regionally localized Sherwood number could be studied in four trusses in the unit cell due to aid of additive manufacturing and the naphthalene sublimation technique. A hot wire is also used to measure the local, unsteady velocity at several points downstream of the unit cell. This data is used as a complement to the mass transfer data.

Due to the orientation in the wind tunnel, trusses 1 and 3 are better compared to a cylinder in crossflow. Both trusses exhibit better transfer than cylinder in the whole Reynolds number range. Truss 2, despite the orientation in the wind tunnel, consistently gets better transfer than cylinder at $Re \geq 900$ and even truss 4 consistently gets better transfer than a cylinder at $Re \geq 1200$. As the Reynolds number increases, each truss' percent increase from a cylinder gets larger. Overall trusses 1 and 3 perform similarly to their counterpart in a single unit cell. Truss 2 at $Re \geq 900$ gets slightly better transfer than its counterpart in the single unit cell and truss 4 gets slightly worse transfer in the entirety of the Reynolds number range. Despite some differences in specific trusses, overall, the center unit cell gets similar Sherwood numbers to a single unit cell and improves transfer by 5–37% compared to a cylinder. Due to the orientation in the wind tunnel, trusses 2 and 4 are compared to turbulent and flat plate correlations. The trusses get significantly better heat transfer than both flat plate correlations except at around $Re = 670$. Truss 4 especially gets a significant increase in heat transfer compared to a turbulent and laminar flat plate with a 178–228% increase.

ACKNOWLEDGMENTS

This project was supported by the Department of Energy's Kansas City National Security Campus.

REFERENCES

[1] H. J. Xu, Z. G. Qu, T. J. Lu, Y. L. He, and W. Q. Tao. Thermal modeling of forced convection in a parallel-plate channel partially filled with metallic foams. *Journal of Heat Transfer*, 133(9), jul 2011. doi: 10.1115/1.4004209.

[2] Henk Huisseune, Sven De Schampheleire, Bernd Ameel, and Michel De Paepe. Comparison of metal foam heat exchangers to a finned heat exchanger for low reynolds number applications. *International Journal of Heat and Mass Transfer*, 89:1–9, oct 2015. doi: 10.1016/j.ijheatmasstransfer.2015.05.013.

[3] Chih-Cheng Chen, Po-Chuan Huang, and Hsiu-Ying Hwang. Enhanced forced convective cooling of heat sources by metal-foam porous layers. *International Journal of Heat and Mass Transfer*, 58(1-2):356–373, mar 2013. doi: 10.1016/j.ijheatmasstransfer.2012.11.041.

[4] Mo Bai and J.N. Chung. Analytical and numerical prediction of heat transfer and pressure drop in open-cell metal foams. *International Journal of Thermal Sciences*, 50(6):869–880, jun 2011. doi: 10.1016/j.ijthermalsci.2011.01.007.

[5] A. Tamayol and K. Hooman. Thermal assessment of forced convection through metal foam heat exchangers. *Journal of Heat Transfer*, 133(11), sep 2011. doi: 10.1115/1.4004530.

[6] Shadi Mahjoob and Kambiz Vafai. A synthesis of fluid and thermal transport models for metal foam heat exchangers. *International Journal of Heat and Mass Transfer*, 51 (15-16):3701–3711, jul 2008. doi: 10.1016/j.ijheatmasstransfer.2007.12.012.

[7] W. Lu, C.Y. Zhao, and S.A. Tassou. Thermal analysis on metal-foam filled heat exchangers. part i: Metal-foam filled pipes. *International Journal of Heat and Mass Transfer*, 49(15-16):2751–2761, jul 2006. doi: 10.1016/j.ijheatmasstransfer.2005.12.012.

[8] C.Y. Zhao, W. Lu, and S.A. Tassou. Thermal analysis on metal-foam filled heat exchangers. part II: Tube heat exchangers. *International Journal of Heat and Mass Transfer*, 49(15-16):2762–2770, jul 2006. doi: 10.1016/j.ijheatmasstransfer.2005.12.014.

[9] J.-J. Hwang, G.-J. Hwang, R.-H. Yeh, and C.-H. Chao. Measurement of interstitial convective heat transfer and frictional drag for flow across metal foams. *Journal of Heat Transfer*, 124(1):120–129, may 2001. doi: 10.1115/1.1416690.

[10] V. V. Calmidi and R. L. Mahajan. Forced convection in high porosity metal foams. *Journal of Heat Transfer*, 122(3):557–565, feb 2000. doi: 10.1115/1.1287793.

[11] John Banhart. Manufacture, characterisation and application of cellular metals and metal foams. *Progress in Materials Science*, 46(6):559–632, jan 2001. doi: 10.1016/S0079-6425(00)00002-5.

[12] Burhan Ozmat, Bryan Leyda, and Burton Benson. Thermal applications of open-cell metal foams. *Materials and Manufacturing Processes*, 19(5):839–862, oct 2004. doi: 10.1081/LMMP-200030568.

[13] Uzair Sajjad, Tauseef ur Rehman, Mubasher Ali, Cheol Woo Park, and Wei-Mon Yan. Manufacturing and potential applications of lattice structures in thermal systems: A comprehensive review of recent advances. *International Journal of Heat and Mass Transfer*, 198:123352, dec 2022. doi: 10.1016/j.ijheatmasstransfer.2022.123352.

[14] Inderjot Kaur and Prashant Singh. Critical evaluation of additively manufactured metal lattices for viability in advanced heat exchangers. *International Journal of Heat and Mass Transfer*, 168:120858, apr 2021. doi: 10.1016/j.ijheatmasstransfer.2020.120858.

[15] T. Kim, C.Y. Zhao, T.J. Lu, and H.P. Hodson. Convective heat dissipation with lattice-frame materials. *Mechanics of Materials*, 36(8):767–780, aug 2004. doi: doi:10.1016/j.mechmat.2003.07.001.

[16] T. Kim, H.P. Hodson, and T.J. Lu. Contribution of vortex structures and flow separation to local and overall pressure and heat transfer characteristics in an ultralightweight lattice material. *International Journal of Heat and Mass Transfer*, 48(19-20):4243–4264, sep 2005. doi: 10.1016/j.ijheatmasstransfer.2005.04.026.

[17] Beibei Shen, Yang Li, Hongbin Yan, Sandra K.S. Boetcher, and Gongnan Xie. Heat transfer enhancement of wedge-shaped channels by replacing pin fins with kagome lattice structures. *International Journal of Heat and Mass Transfer*, 141:88–101, oct 2019. doi: 10.1016/j.ijheatmasstransfer.2019.06.059.

[18] Liang Xu, Hanghang Chen, Lei Xi, Yanhong Xiong, Jianmin Gao, and Yunlong Li. Flow and heat transfer characteristics of a staggered array of kagome lattice structures in rectangular channels. *Heat and Mass Transfer*, 58(1):41–64, jun 2021. doi: 10.1007/s00231-021-03100-2.

[19] Beibei Shen, Hongbin Yan, Hongqian Xue, and Gongnan Xie. The effects of geometrical topology on fluid flow and thermal performance in kagome cored sandwich panels. *Applied Thermal Engineering*, 142:79–88, sep 2018. doi: 10.1016/j.applthermaleng.2018.06.080.

[20] H.B. Yan, Q.C. Zhang, T.J. Lu, and T. Kim. A lightweight x-type metallic lattice in single-phase forced convection. *International Journal of Heat and Mass Transfer*, 83: 273–283, apr 2015. doi: 10.1016/j.ijheatmasstransfer.2014.11.061.

[21] H.B. Yan, Q.C. Zhang, and T.J. Lu. Heat transfer enhancement by x-type lattice in ventilated brake disc. *International Journal of Thermal Sciences*, 107:39–55, sep 2016. doi: 10.1016/j.ijthermalsci.2016.03.026.

[22] Lei Xi, Liang Xu, Jianmin Gao, Zhen Zhao, and Yunlong Li. Study on flow and heat transfer performance of x-type truss array cooling channel. *Case Studies in Thermal Engineering*, 26:101034, aug 2021. doi: 10.1016/j.csite.2021.101034.

[23] J.Y. Ho, K.C. Leong, and T.N. Wong. Additively-manufactured metallic porous lattice heat exchangers for air-side heat transfer enhancement. *International Journal of Heat and Mass Transfer*, 150:119262, apr 2020. doi: 10.1016/j.ijheatmasstransfer.2019.119262.

[24] Dong Liang, Guanlin He, Wei Chen, Yaoqi Chen, and Minking K. Chyu. Fluid flow and heat transfer performance for micro-lattice structures fabricated by selective laser melting. *International Journal of Thermal Sciences*, 172:107312, feb 2022. doi: 10.1016/j.ijthermalsci.2021.107312.

[25] Justin Broughton and Yogendra K. Joshi. Comparison of single-phase convection in additive manufactured versus traditional metal foams. *Journal of Heat Transfer*, 142 (8), jun 2020. doi: 10.1115/1.4046972.

[26] R.J. Goldstein and H.H. Cho. A review of mass transfer measurements using naphthalene sublimation. *Experimental Thermal and Fluid Science*, 10(4):416–434, may 1995. doi: https://doi.org/10.1016/0894-1777(94)00071-F.

[27] D. Ambrose, I.J. Lawrenson, and C.H.S. Sprake. The vapour pressure of naphthalene. *The Journal of Chemical Thermodynamics*, 7(12):1173–1176, dec 1975. doi: 10.1016/0021-9614(75)90038-5.

[28] Cho Keumnam, Thomas F. Irvine, and Jacob Karni. Measurement of the diffusion coefficient of naphthalene into air. *International Journal of Heat and Mass Transfer*, 35(4):957–966, apr 1992. doi: 10.1016/0017-9310(92)90260-Y.

[29] S. W. Churchill and M. Bernstein. A correlating equation for forced convection from gases and liquids to a circular cylinder in crossflow. *Journal of Heat Transfer*, 99(2): 300–306, may 1977. doi: 10.1115/1.3450685.

[30] Frank P. Incropera. *Fundamentals of heat and mass transfer.* Wiley, sixth edition, 2006. ISBN 9780471457282.

SECTION

3. UNPUBLISHED CONTENT

3.1. TURBULENCE INTENSITY AND INTEGRAL LENGTH SCALES DOWNSTREAM OF MESHES

The idea behind this additional effort was to test the effect of turbulence intensity and integral length scales on mass transfer off a cylinder and potentially the unit cell geometries. The first part of this experiment is to verify the turbulence intensity and integral length scales behind various sized meshes by comparing the experimental results to Roach [22] correlations. Custom sized meshes are first created and printed with dimensions shown in Table 3.1. Several biplanar stainless steel (SS) meshes are then bought and then those meshes are copied and printed using additive manufacturing in both biplanar and coplanar forms. These sizes are shown in Table 3.2 Although the entirety of the experiment is not complete, some results were analyzed, and they are shown below.

Table 3.1. Custom created mesh sizes (M and d in mm).

M	d	M/d
21	7.5	2.8
48	16	3
16	4	4
32	6	5.3
47	7.5	6.3

3.1.1. Integral Length Scales. The larger diameter mesh integral length scale results are shown in Figure 3.1. It was observed that the larger diameter on the meshes appeared to have an effect on the integral length scales. It is possible the integral lengths scales are being dampened due to the ratio of the wind tunnel cross sectional area to the diameter of the meshes. The SS meshes and their counterpart are shown in Figure 3.2.

Table 3.2. SS meshes' and their printed counterparts' sizes (M and d in mm).

M	d	M/d
8.46	1.19	7.09
12.7	1.19	7.94
25.4	2.03	12.5

Overall, the SS versions don't produce the same integral length scales as the printed versions. The rough surface of the plastic printed meshes could also be affecting the results. The results are also very scattered around Roach's correlation. The printed biplanar and coplanar mesh comparisons are shown in Figure 3.3. In all scenarios, the coplanar and biplanar integral length scales are different which would mean having the perpendicular mesh cylinders on a different plane changes the integral length scales. There is also large scatter if comparing them all to Roach's correlation.

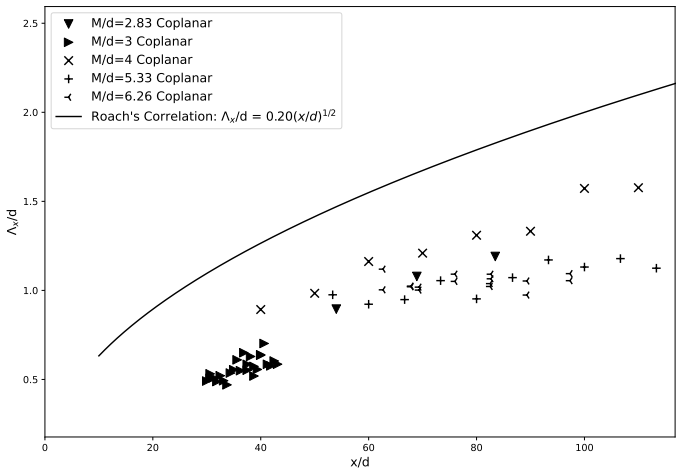

Figure 3.1. Integral length scales of various large diameter meshes.

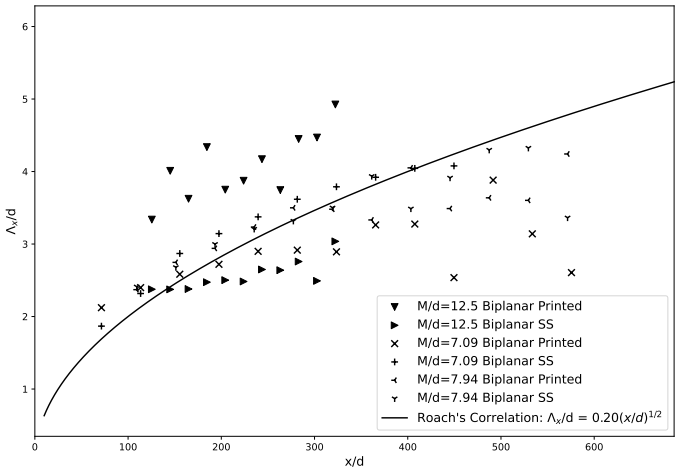

Figure 3.2. Integral length scales comparison between biplanar SS and printed meshes.

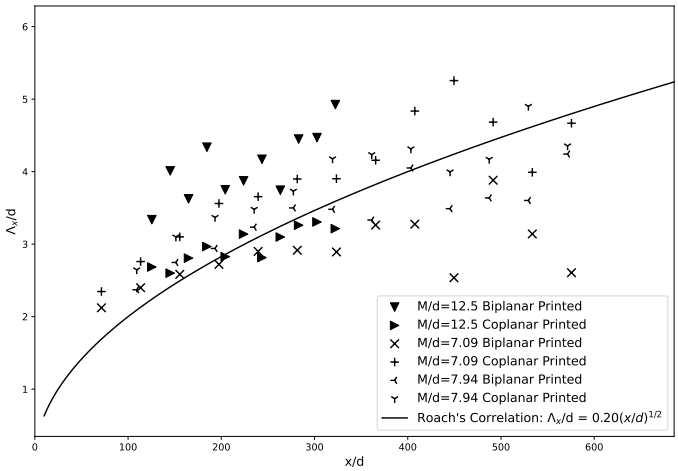

Figure 3.3. Integral length scales comparison between coplanar and biplanar printed meshes.

3.1.2. Turbulence Intensity. The turbulence intensity is also obtained to see if there are any differences among the same scenarios. Figure 3.4 shows the effect of diameter. In all cases, except the $M/d = 2.83$, the turbulence intensity is higher than Roach's correlation. It seems the larger diameter is affecting both the integral length scales and turbulence intensity. Figure 3.5 shows the comparison between the SS version and printed version of the meshes. Each mesh follows the same Roach trend, but it seems as M/d increase, the error compared to Roach's correlation increases. Figure 3.6 shows the comparison between the coplanar and biplanar version of the meshes. The $M/d = 12.5$ coplanar

and biplanar meshes produce similar turbulence intensity. as well as the $M/d = 7.94$. Out of the three sizes, the $M/d = 7.09$ meshes have the biggest difference between the two types.

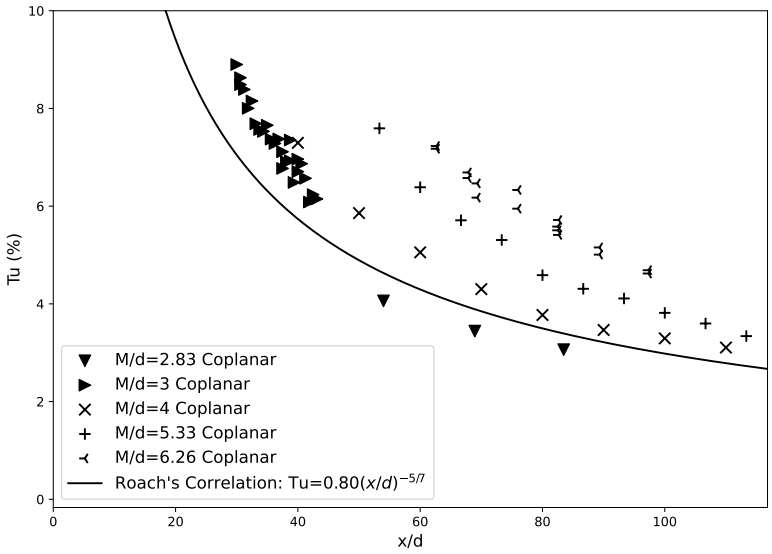

Figure 3.4. Turbulence intensity of various large diameter meshes.

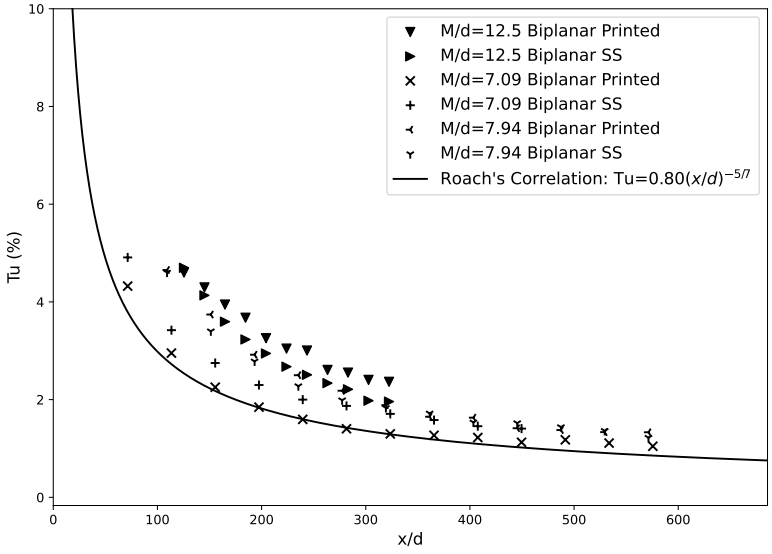

Figure 3.5. Turbulence intensity comparison between biplanar SS and printed meshes.

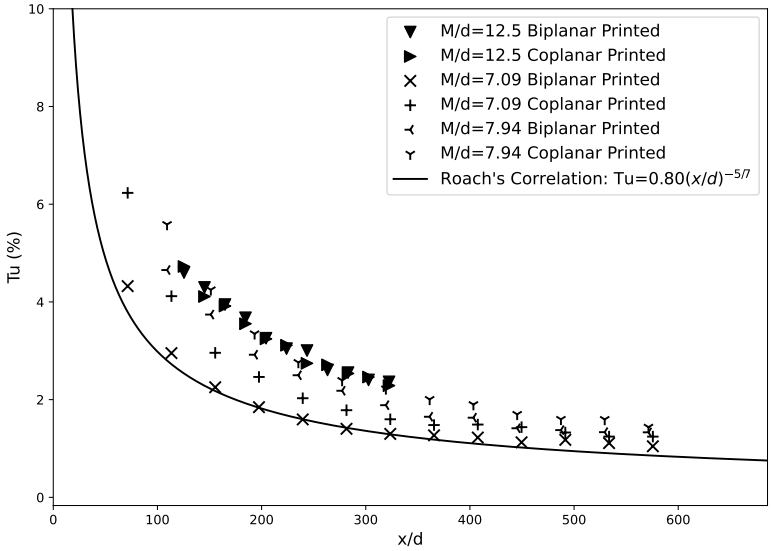

Figure 3.6. Turbulence intensity comparison between coplanar and biplanar printed meshes.

Due to the drastic differences between Roach's correlation and the experimental results especially for the custom, larger diameter meshes and time, the entirety of the experiment could not be completed. An appropriate next step would be to see how turbulence intensity and integral length scales affect transport coefficients.

4. SUMMARY AND CONCLUSIONS

4.1. SUMMARY

This research investigated the partially localized and area average transfer coefficient over a 300–1800 Reynolds number range in several unit cell configurations using a combination of AM parts and the naphthalene sublimation technique. The configurations include a single unit cell, two unit cells in series, three unit cells in series, and a 3x3 unit cell array. Hot wire anemometry measurements are also taken to supplement the mass transfer measurements.

Paper I examines the single unit cell and the unit cells in series. In the single unit cell, the upstream and downstream trusses exhibit a 30–109% increase in Sherwood number compared to a turbulent flat plate and 16–42% increase in Sherwood number based on diameter compared to a circular cylinder in crossflow over the Reynolds number range. The downstream truss on the downstream coated unit cell for the two-in-series configuration shows a 108–169% increase in Sherwood number compared to a turbulent flat plate and if comparing the area average Sherwood number of the downstream unit cell based on the diameter to a cylinder in crossflow, then it gets a 12–29% increase which is a slight decrease in performance compared to the single unit cell. The three unit cells in series configurations downstream truss on the downstream unit cell gets 130–196% better transfer than a turbulent flat plate. Overall, the downstream unit cell on the three in series performs similarly to the downstream unit cell in the two in series configuration with a 16–29% increase over the Reynolds number range.

Paper II looks at the area average transfer in the center unit cell in a 3x3 unit cell array. Treating the upstream and downstream trusses on the center unit cell as a flat plate leads to a 37–63% and 178–228% increase over a turbulent flat plate. The overall Sherwood number based on the diameter of the naphthalene coated parts in the center unit cell is getting

a 5–37% increase compared to a cylinder in crossflow. Comparing the overall Sherwood numbers between the single unit cell and the central unit cell in the array, the performance is similar; however, the trusses along the z-axis in the array are getting slightly higher Sherwood numbers in the higher end of the Reynolds number range and a slight decrease in Sherwood numbers in the upstream and downstream trusses.

4.2. RECOMMENDATIONS FOR FUTURE RESEARCH

Future research should involve studying the effect of changing the parameters of the unit cell geometry. Some parameter changes should include increasing or decreasing L/D, rotating the geometry in a wind tunnel, and adding more trusses. The geometry could be optimized for the best heat transfer enhancement by investigating the different parameters. A more localized Sherwood number or Nusselt number would be essential in determining the best parameters for the unit cell by studying the localized effect of the changing parameters. To provide a supplement to this work, a more detailed flow analysis should be performed by using computation fluid dynamics and observing the various flow structures and the effect these have on the localized heat transfer.

More configurations with the same unit cell topology should be researched including more unit cells in series (4, 5, etc) and also combining the unit cell array 'wall' with unit cells in series. Having multiple arrays in series could be beneficial by simulating a channel filled with this studied unit cell topology. In addition to more configurations, sandwich panels with this topology should be constructed to show the real world applications in heat exchangers. In combination with the sandwich panel, the pressure drop across them should also be studied to possibly show if these provide a favorable pressure drop or if they should be refined to provide a favorable pressure drop.

This study observed the heat transfer at the lower Reynolds number range, but future studies should also look at the higher Reynolds number ranges to see if this geometry can work more efficiently at these higher Reynolds number ranges.

REFERENCES

[1] D. Ambrose, I.J. Lawrenson, and C.H.S. Sprake. The vapour pressure of naphthalene. *The Journal of Chemical Thermodynamics*, 7(12):1173–1176, dec 1975. doi: 10.1016/0021-9614(75)90038-5.

[2] Mo Bai and J.N. Chung. Analytical and numerical prediction of heat transfer and pressure drop in open-cell metal foams. *International Journal of Thermal Sciences*, 50(6):869–880, jun 2011. doi: 10.1016/j.ijthermalsci.2011.01.007.

[3] John Banhart. Manufacture, characterisation and application of cellular metals and metal foams. *Progress in Materials Science*, 46(6):559–632, jan 2001. doi: 10.1016/S0079-6425(00)00002-5.

[4] Justin Broughton and Yogendra K. Joshi. Comparison of single-phase convection in additive manufactured versus traditional metal foams. *Journal of Heat Transfer*, 142 (8), jun 2020. doi: 10.1115/1.4046972.

[5] V. V. Calmidi and R. L. Mahajan. Forced convection in high porosity metal foams. *Journal of Heat Transfer*, 122(3):557–565, feb 2000. doi: 10.1115/1.1287793.

[6] Aniket Chaudhari, Pawankumar Ekade, and Shankar Krishnan. Experimental investigation of heat transfer and fluid flow in octet-truss lattice geometry. *International Journal of Thermal Sciences*, 143:64–75, sep 2019. doi: 10.1016/j.ijthermalsci.2019.05.003.

[7] Chih-Cheng Chen, Po-Chuan Huang, and Hsiu-Ying Hwang. Enhanced forced convective cooling of heat sources by metal-foam porous layers. *International Journal of Heat and Mass Transfer*, 58(1-2):356–373, mar 2013. doi: 10.1016/j.ijheatmasstransfer.2012.11.041.

[8] S. W. Churchill and M. Bernstein. A correlating equation for forced convection from gases and liquids to a circular cylinder in crossflow. *Journal of Heat Transfer*, 99(2): 300–306, may 1977. doi: 10.1115/1.3450685.

[9] R.J. Goldstein and H.H. Cho. A review of mass transfer measurements using naphthalene sublimation. *Experimental Thermal and Fluid Science*, 10(4):416–434, may 1995. doi: https://doi.org/10.1016/0894-1777(94)00071-F.

[10] J.Y. Ho, K.C. Leong, and T.N. Wong. Additively-manufactured metallic porous lattice heat exchangers for air-side heat transfer enhancement. *International Journal of Heat and Mass Transfer*, 150:119262, apr 2020. doi: 10.1016/j.ijheatmasstransfer.2019.119262.

[11] Henk Huisseune, Sven De Schampheleire, Bernd Ameel, and Michel De Paepe. Comparison of metal foam heat exchangers to a finned heat exchanger for low reynolds number applications. *International Journal of Heat and Mass Transfer*, 89:1–9, oct 2015. doi: 10.1016/j.ijheatmasstransfer.2015.05.013.

[12] J.-J. Hwang, G.-J. Hwang, R.-H. Yeh, and C.-H. Chao. Measurement of interstitial convective heat transfer and frictional drag for flow across metal foams. *Journal of Heat Transfer*, 124(1):120–129, may 2001. doi: 10.1115/1.1416690.

[13] Frank P. Incropera. *Fundamentals of heat and mass transfer.* Wiley, sixth edition, 2006. ISBN 9780471457282.

[14] Inderjot Kaur and Prashant Singh. Critical evaluation of additively manufactured metal lattices for viability in advanced heat exchangers. *International Journal of Heat and Mass Transfer*, 168:120858, apr 2021. doi: 10.1016/j.ijheatmasstransfer.2020.120858.

[15] Cho Keumnam, Thomas F. Irvine, and Jacob Karni. Measurement of the diffusion coefficient of naphthalene into air. *International Journal of Heat and Mass Transfer*, 35(4):957–966, apr 1992. doi: 10.1016/0017-9310(92)90260-Y.

[16] T. Kim, C.Y. Zhao, T.J. Lu, and H.P. Hodson. Convective heat dissipation with lattice-frame materials. *Mechanics of Materials*, 36(8):767–780, aug 2004. doi: doi:10.1016/j.mechmat.2003.07.001.

[17] T. Kim, H.P. Hodson, and T.J. Lu. Contribution of vortex structures and flow separation to local and overall pressure and heat transfer characteristics in an ultralightweight lattice material. *International Journal of Heat and Mass Transfer*, 48(19-20):4243–4264, sep 2005. doi: 10.1016/j.ijheatmasstransfer.2005.04.026.

[18] Dong Liang, Guanlin He, Wei Chen, Yaoqi Chen, and Minking K. Chyu. Fluid flow and heat transfer performance for micro-lattice structures fabricated by selective laser melting. *International Journal of Thermal Sciences*, 172:107312, feb 2022. doi: 10.1016/j.ijthermalsci.2021.107312.

[19] W. Lu, C.Y. Zhao, and S.A. Tassou. Thermal analysis on metal-foam filled heat exchangers. part i: Metal-foam filled pipes. *International Journal of Heat and Mass Transfer*, 49(15-16):2751–2761, jul 2006. doi: 10.1016/j.ijheatmasstransfer.2005.12.012.

[20] Shadi Mahjoob and Kambiz Vafai. A synthesis of fluid and thermal transport models for metal foam heat exchangers. *International Journal of Heat and Mass Transfer*, 51 (15-16):3701–3711, jul 2008. doi: 10.1016/j.ijheatmasstransfer.2007.12.012.

[21] Burhan Ozmat, Bryan Leyda, and Burton Benson. Thermal applications of open-cell metal foams. *Materials and Manufacturing Processes*, 19(5):839–862, oct 2004. doi: 10.1081/LMMP-200030568.

[22] P.E. Roach. The generation of nearly isotropic turbulence by means of grids. *International Journal of Heat and Fluid Flow*, 8(2):82–92, jun 1987. doi: 10.1016/0142-727X(87)90001-4.

[23] Uzair Sajjad, Tauseef ur Rehman, Mubasher Ali, Cheol Woo Park, and Wei-Mon Yan. Manufacturing and potential applications of lattice structures in thermal systems: A comprehensive review of recent advances. *International Journal of Heat and Mass Transfer*, 198:123352, dec 2022. doi: 10.1016/j.ijheatmasstransfer.2022.123352.

[24] Beibei Shen, Hongbin Yan, Hongqian Xue, and Gongnan Xie. The effects of geometrical topology on fluid flow and thermal performance in kagome cored sandwich panels. *Applied Thermal Engineering*, 142:79–88, sep 2018. doi: 10.1016/j.applthermaleng.2018.06.080.

[25] Beibei Shen, Yang Li, Hongbin Yan, Sandra K.S. Boetcher, and Gongnan Xie. Heat transfer enhancement of wedge-shaped channels by replacing pin fins with kagome lattice structures. *International Journal of Heat and Mass Transfer*, 141:88–101, oct 2019. doi: 10.1016/j.ijheatmasstransfer.2019.06.059.

[26] A. Tamayol and K. Hooman. Thermal assessment of forced convection through metal foam heat exchangers. *Journal of Heat Transfer*, 133(11), sep 2011. doi: 10.1115/1.4004530.

[27] Lei Xi, Liang Xu, Jianmin Gao, Zhen Zhao, and Yunlong Li. Study on flow and heat transfer performance of x-type truss array cooling channel. *Case Studies in Thermal Engineering*, 26:101034, aug 2021. doi: 10.1016/j.csite.2021.101034.

[28] H. J. Xu, Z. G. Qu, T. J. Lu, Y. L. He, and W. Q. Tao. Thermal modeling of forced convection in a parallel-plate channel partially filled with metallic foams. *Journal of Heat Transfer*, 133(9), jul 2011. doi: 10.1115/1.4004209.

[29] Liang Xu, Hanghang Chen, Lei Xi, Yanhong Xiong, Jianmin Gao, and Yunlong Li. Flow and heat transfer characteristics of a staggered array of kagome lattice structures in rectangular channels. *Heat and Mass Transfer*, 58(1):41–64, jun 2021. doi: 10.1007/s00231-021-03100-2.

[30] H.B. Yan, Q.C. Zhang, T.J. Lu, and T. Kim. A lightweight x-type metallic lattice in single-phase forced convection. *International Journal of Heat and Mass Transfer*, 83: 273–283, apr 2015. doi: 10.1016/j.ijheatmasstransfer.2014.11.061.

[31] H.B. Yan, Q.C. Zhang, and T.J. Lu. Heat transfer enhancement by x-type lattice in ventilated brake disc. *International Journal of Thermal Sciences*, 107:39–55, sep 2016. doi: 10.1016/j.ijthermalsci.2016.03.026.

[32] C.Y. Zhao, W. Lu, and S.A. Tassou. Thermal analysis on metal-foam filled heat exchangers. part II: Tube heat exchangers. *International Journal of Heat and Mass Transfer*, 49(15-16):2762–2770, jul 2006. doi: 10.1016/j.ijheatmasstransfer.2005.12.014.

VITA

Benjamin Gabriel Mackey was born in St. Louis Missouri in 1996. In 2015, he began attending the University of Kansas and received his Bachelor of Science degree in Petroleum Engineering in 2019. In 2020, he began pursuing his Master of Science degree in Mechanical Engineering under Dr. Kelly O. Homan and received it in July 2023 from Missouri S&T.